Quantifying the Impacts of Marine Aerosols over the Southeast Atlantic Ocean using a chemical transport model: Implications for aerosol-cloud interactions

Mashiat Hossain[1], Rebecca M. Garland[2], Hannah M. Horowitz[1]

[1] Civil and Environmental Engineering, University of Illinois Urbana-Champaign, IL, USA
[2] Department of Geography, Geoinformatics and Meteorology, University of Pretoria, Pretoria, South Africa

Correspondence to: Mashiat Hossain (mashiat3@illinois.edu), Hannah M. Horowitz (hmhorow@illinois.edu)

Abstract. The southeast Atlantic region, characterized by persistent stratocumulus clouds, has one of the highest uncertainties in aerosol radiative forcing and significant variability across climate models. In this study, we analyze the seasonally varying role of marine aerosol sources and identify key uncertainties in aerosol composition at cloud-relevant altitudes over the southeast Atlantic using the GEOS-Chem chemical transport model. We evaluate simulated aerosol optical depth (AOD) and speciated aerosol concentrations against those collected from ground observations and aircraft campaigns such as LASIC, ORACLES, and CLARIFY, conducted during 2017. The model consistently underestimates AOD relative to AERONET, particularly at remote locations like Ascension Island. However, when compared with aerosol mass concentrations from aircraft campaigns during the biomass burning period, it performs adequately at cloud-relevant altitudes, with a normalized mean bias (NMB) between -3.5% (CLARIFY) and -7.5% (ORACLES). At these altitudes, in the model organic aerosols (63%) dominate during the biomass burning period, while sulfate (41%) prevails during austral summer, when dimethylsulfide (DMS) emissions peak in the model. Our findings indicate that marine sulfate can account for up to 69% of total sulfate during high DMS period. Sensitivity analyses indicate that refining DMS emissions and oxidation chemistry may increase sulfate aerosol produced from marine sources, highlighting that there remains large uncertainty in the role of DMS emissions in the marine boundary layer. Additionally, we find marine primary organic aerosol emissions may substantially increase total organic aerosol concentrations, particularly during austral summer. This study underscores the imperative need to refine marine emissions and their chemical transformations, as aerosols from marine sources are a major component of total aerosols at cloud-relevant altitudes and may impact uncertainties in aerosol radiative forcing over the southeast Atlantic.

1 Introduction

Marine aerosols are a primary contributor to natural atmospheric aerosols, and consequently influence the Earth's radiative balance (Spracklen et al., 2008; Vignati et al., 2001). Aerosols in the marine boundary layer have significant impact on the properties of low-altitude marine clouds, particularly their ability to reflect solar radiation and cool the climate (Seinfeld and Pandis, 2016; Wood, 2012; Chen et al., 2014; Quinn et al., 2017). The southeast Atlantic (SEA) is marked by a persistent deck of low-level stratocumulus (Sc) clouds. However, this region exhibits highest uncertainty in aerosol radiative forcings in the AeroCom intercomparison across CMIP5 general circulation models (GCMs) and chemical transport models (Stier et al., 2013). This uncertainty is primarily driven by challenges in

34   accurately representing cloud fraction, aerosol-cloud properties, and vertical structure, both in the presence and

35   absence of smoke (Stier et al., 2013; Doherty et al., 2022). In this study, we investigate the role of marine aerosols

36   and sources of uncertainty affecting aerosol composition within the boundary layer, particularly in this critical region

37   of aerosol-cloud interactions over the SEA.

38   The SEA region encompasses the Benguela upwelling system (BUS), renowned for its high primary production of

39   marine phytoplankton and fish populations (Shannon and Nelson, 1996; Jarre et al., 2015). This elevated

40   phytoplankton activity serves as the main natural source of the volatile organic compound dimethylsulfide (DMS),

41   thereby influencing the global tropospheric sulfur budget (Andreae, 1990; Bates et al., 1992). Once released into the

42   atmosphere through air-sea exchange, DMS undergoes complex chemical transformations. In the gas phase, it is

43   oxidized to form H_2SO_4 and methanesulfonic acid (MSA), which has implications for new particle formation (Chen

44   et al., 2015); while in the aqueous phase, it leads to the production of MSA and sulfate aerosols, impacting cloud

45   microphysical properties (Kaufman and Tanré, 1994). Although DMS is a critical source of natural aerosols,

46   contributing over 50% of natural gas-phase sulfur emissions (Chin et al., 1996; Kilgour et al., 2021), the exact

47   mechanisms of DMS oxidation and subsequent formation of sulfate and MSA aerosol remain inadequately understood

48   (Ravishankara et al., 1997; Barnes et al., 2006; Hoffmann et al., 2016). This gap in understanding contributes to

49   substantial uncertainty in aerosol radiative forcing, which is highly sensitive to uncertainties in natural aerosols

50   (Carslaw et al., 2013; Fung et al., 2022). Additionally, marine aerosols comprise primary aerosols such as sea spray

51   aerosols, which consist of salts, sulfate, and organic matter, released into the atmosphere primarily by the bubble-

52   bursting process (O'Dowd and De Leeuw, 2007; Russell et al., 2010; Prather et al., 2013; Brooks and Thornton, 2018;

53   Russell et al., 2023). Investigating the uncertainties related to marine emissions and chemistry are crucial to refine our

54   understanding of the impacts of marine aerosols on climate.

55   The SEA lies at the confluence of not only marine aerosols, but other natural and anthropogenic aerosols from local

56   and distant origin (Andreae et al., 1995; Swap et al., 1996; Formenti et al., 1999; Swap et al., 2003; Tournadre, 2014).

57   During the austral spring (August to October), seasonal fires in the neighboring southern African region contribute

58   nearly one-third of global total biomass burning emissions (van der Werf et al., 2010). This seasonal influx of biomass

59   burning aerosols aloft interacts with the underlying Sc deck, introducing considerable variability into aerosol forcing

60   assessments in the SEA region (Lindesay et al., 1996; Swap et al., 2003). To address these uncertainties, several

61   international field campaigns were conducted between 1992 and 2018 during the peak biomass burning season (Swap

62   et al., 2003; Formenti et al., 2019; Haywood et al., 2021; Redemann et al., 2021). Despite the region being a prolific

63   source of marine aerosols throughout the year, the potential impact of aerosols on regional climate dynamics through

64   interactions with the persistent low-level marine clouds outside of the biomass burning season has been largely

65   overlooked.

66   Here, we use the GEOS-Chem global chemical transport model to analyze high-resolution, seasonally varying aerosol

67   composition at the altitudes of persistent stratocumulus clouds over the SEA. We specifically focus on the role of

68   marine aerosols, analyzing their contributions to sulfate and organic aerosol concentrations. We evaluate simulated

aerosol optical depth (AOD) and speciated aerosol concentrations against observational data from the Aerosol Robotic Network (AERONET) and the Layered Atlantic Smoke Interactions with Clouds (LASIC; Zuidema et al., 2018), ObseRvations of Aerosols above CLouds and their intEractionS (ORACLES; Redemann et al., 2021), and CLoud–Aerosol–Radiation Interaction and Forcing (CLARIFY; Haywood et al., 2021) field campaigns during the year 2017. We assess the sensitivity of our results to uncertainty in DMS oxidation mechanisms and emissions of DMS, SO_2, and marine primary organics. Our findings aim to enhance understanding of the seasonally varying role of marine aerosols in aerosol-cloud interactions in the SEA by a comprehensive evaluation of aerosol composition at cloud altitudes.

2 Methodology

2.1 Model Description

Here, we use the GEOS-Chem 3D atmospheric chemical transport model version 13.3.3 with detailed gas- and aerosol-phase tropospheric chemistry (https://zenodo.org/records/5748260). The model is driven by meteorology from the Modern-Era Retrospective Analysis for Research and Applications, Version-2 (MERRA2) reanalysis, from the NASA Global Modeling Assimilation Office (GMAO) (Gelaro et al., 2017). We perform nested grid simulations over the southwestern coast of Africa (40°W-20°E, 0-40°S) with a horizontal resolution of 0.5° by 0.625° and extending over 47 vertical layers from the surface to 0.01hPa. A chemical time step of 20 minutes and transport time step of 10 minutes is applied, as recommended by Philip et al. (2016). Prior to the target year, 2017, we conduct a 6-month spin-up simulation. Boundary conditions are obtained from global simulations performed at 4° latitude × 5° longitude horizontal resolution for the same year after a 6-month initialization.

In GEOS-Chem, carbonaceous aerosol includes organic aerosols (OA) and black carbon (BC). Organic aerosol is simulated using the "simple" scheme which treats primary organic aerosol (POA) as non-volatile and includes irreversible direct yield of SOA from precursors (Pai et al., 2020). The BC simulation follows the methodologies of Park et al. (2003) and Wang et al. (2014). Sulfate (Alexander et al., 2009), nitrate (Jaeglé et al., 2018), and ammonium (Fountoukis and Nenes, 2007) thermodynamic partitioning is estimated using the ISORROPIA II thermodynamic model (Fountoukis and Nenes, 2007). Monthly anthropogenic emissions follow the Community Emissions Data System (CEDSv2) inventory (Hoesly et al., 2018). Biomass burning emissions are calculated using the Global Fire Emissions Database (GFED4.1s) at 0.25°×0.25° spatial resolution, with fractional daily and 3-hourly scaling factors applied to the cumulative monthly data (van der Werf et al., 2017). DMS emissions in the standard model use the Lana et al. (2011) climatology, which compiles DMS concentrations using data from the Global Surface Seawater DMS Database (http://saga.pmel.noaa.gov/dms/) collected from 1972 to 2009, incorporated with additional observations from the South Pacific (Lee et al., 2010). The standard DMS oxidation mechanism in the model includes only three gas-phase DMS reactions, which directly yield SO_2 and MSA according to the reaction mechanism outlined by Chin et al. (1996), and incorporates updated reaction rate coefficients from Burkholder et al. (2015). Sea-salt aerosol (SSA) emissions from the open ocean are both windspeed- (Gong et al., 2003) and sea surface temperature-dependent (Jaeglé et al., 2011). Dust emissions include natural dust (Fairlie et al., 2007) and anthropogenic dust from the AFCID inventory (Philip et al., 2017).

104 In this study, we carry out multiple simulations to explore the sensitivity of marine aerosols to various emission
105 sources. To quantify the impact of marine sources on sulfate aerosols within the stratocumulus cloud layer, we perform
106 a high-resolution (0.5° x 0.625°) marine emissions only sensitivity simulation where SO_2 and SO_4 emissions from
107 anthropogenic sources, biomass burning, volcanic activity, ships and aviation were turned off. Additionally, to
108 investigate the sensitivity of DMS emission fluxes to surface ocean DMS concentrations, we perform an additional
109 simulation with DMS concentrations from Galí et al. (2018). In this dataset, DMS concentrations are estimated through
110 a remote-sensing algorithm that integrates satellite-derived estimates of chlorophyll and light penetration, along with
111 climatological mixed layer depth (Galí et al., 2018). Furthermore, we assess the impact of adding marine POA, co-
112 emitted with sea-salt aerosols (Gantt et al., 2015), on the overall organic aerosol burden, which is not included in the
113 standard model configuration. Finally, to evaluate how uncertainty in biomass burning SO_2 emissions affects the
114 relative importance of marine emissions to sulfate aerosol, we conduct two sets of sensitivity simulations using the
115 Quick Fire Emissions Dataset (QFED) (Darmenov & da Silva, 2013; Das et al., 2017), and the Global Fire
116 Assimilation System (GFAS) (Kaiser et al., 2012; Su et al., 2023). Each of these inventories differ in data sources,
117 methodology, temporal resolution and plume injection height. These sensitivity analyses were conducted for the year
118 2017, following a six-month spin-up period. Details regarding the spatial resolution used in each sensitivity analysis
119 are provided in Table A1.

120 **2.2 Ground-based measurements**

121 We evaluate simulated aerosol optical depth (AOD) against AOD retrieved from the ground-based Aerosol Robotic
122 Network (AERONET) of sun photometers with direct sun measurements every 15 min (Holben et al., 1998). We use
123 Level 2.0 Version 3 data that have improved cloud screening algorithms (Giles et al., 2019). We strategically select
124 nine sites in the study domain along coastal and oceanic regions, as shown in Fig. 1. Site information, including the
125 coordinates, number of months with available data and the monthly average AOD for three distinct time periods, is
126 summarized in Table A2. The AERONET monthly average AOD is computed from daily averages for sites with at
127 least 3 months of observations during the model simulation period (year 2017) and months with at least 15 days of
128 measurements. These are then compared with the monthly mean AOD from the GEOS-Chem model.

129 The modeled AOD is sampled at each AERONET site location and computed at 550 nm wavelength by vertically
130 integrating scattering and absorption coefficients based on the properties of various aerosol components, such as size
131 distributions, hygroscopicity, refractive indices, and densities (Latimer and Martin, 2019). For comparison with
132 modeled monthly AOD, daily measurements at each site at 440 nm are first interpolated to the standard wavelength
133 of 550 nm using the local Ångström exponent between 440 and 870 nm channels, following the Ångström power law
134 (Eq. (1); Martínez-Lozano et al., 1998). These interpolated values are then averaged to calculate the observed mean
135 monthly AOD. The interpolation formula used is:

136 $$AOD_{(550nm)} = AOD_{(440nm)} * \left(\frac{550}{440}\right)^{-\alpha ext\left(\frac{440}{870}\right)} \tag{1}$$

137
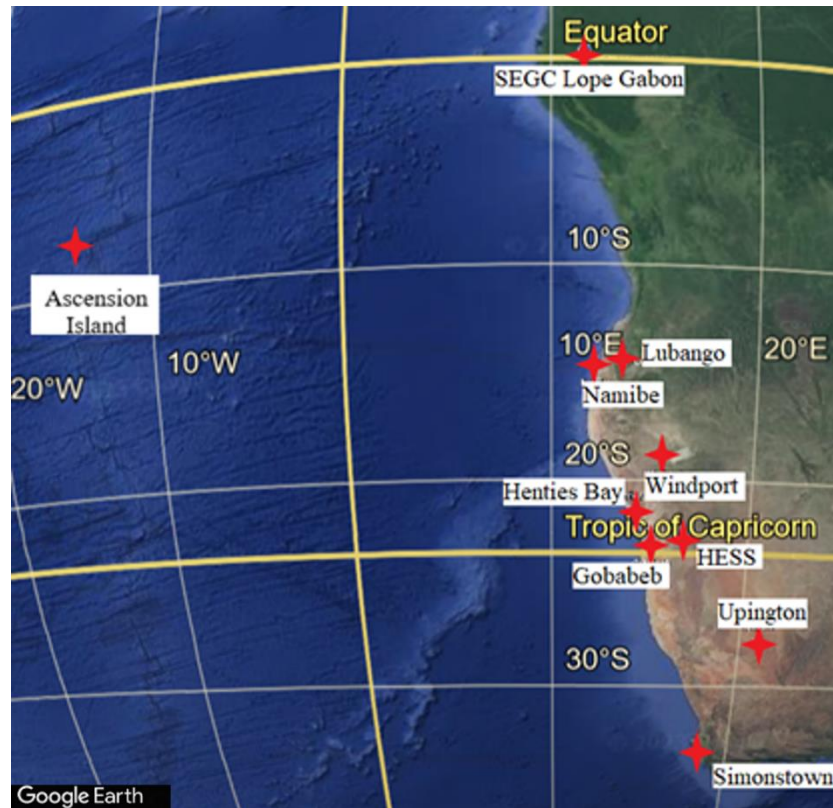
Figure 1: Map of AERONET sites used for model evaluation (© Google Earth).

In addition, we evaluate the model's relative aerosol composition against measurements from the Atmospheric Radiation Measurement (ARM) facility on Ascension Island during the LASIC campaign, conducted from January to November 2017. LASIC employed an Aerodyne aerosol chemical speciation monitor (ACSM) to provide quantitative measurement of the chemical composition of non-refractory aerosol components including sulfate, nitrate, ammonium, and organics. For comparative analysis, we use aerosol concentrations corrected for composition-dependent collection efficiency (CDCE) obtained from the ARM Data Archive. Barrett et al. (2022) reported that aerosol mass concentrations of individual components observed by the LASIC ACSM were 2 to 4.5 times lower than those measured by the aerosol mass spectrometer (AMS) aboard the CLARIFY campaign aircraft. Hence, we evaluate the relative rather than absolute aerosol speciation in GEOS-Chem against the LASIC ACSM.

2.3 Aircraft measurements

We evaluate simulated aerosol composition against airborne measurements from two campaigns, NASA ORACLES (Redemann et al., 2021; Ryoo et al., 2021) and UK CLARIFY (Haywood et al., 2021). The ORACLES field campaign used the NASA P-3 aircraft to make measurements based out of São Tomé and Príncipe while CLARIFY used the FAAM BAe-146 aircraft around Ascension Island for data collection. The ORACLES aircraft primarily conducted morning sampling, between 8:00-13:00 UTC, while the CLARIFY aircraft often sampled extended hours, typically from 7:00-18:00 UTC. Both campaigns occurred during the austral winter/spring (August-September), corresponding

155   with peak biomass burning events in southern Africa (Adebiyi et al., 2015). Figure 2 shows the flight tracks for these

156   campaigns. The primary instruments and references for each campaign are listed in Table 1.

157
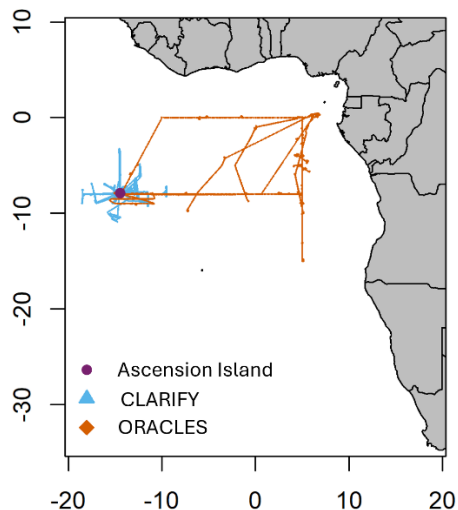
158

159   **Figure 2:** Flight tracks from the two aircraft campaigns used to evaluate the model, CLARIFY (in blue) and ORACLES (in orange),

160   conducted during August-September 2017 over the southeast Atlantic region. Ascension Island is marked by the purple dot.

161   To facilitate comparison between airborne measurements and the GEOS-Chem model, we sampled the model to the

162   nearest grid box, both temporally and spatially, along the flight tracks. Observations from both campaigns are reported

163   at 1-minute averaging intervals, while the model operates at a 10-minute temporal resolution (see Sect. 2.1). Aerosol

164   concentrations from the campaigns are reported as mass concentrations at standard temperature and pressure (STP:

165   273 K, 1 atm). The modeled concentrations are thus also standardized to STP conditions.

166   **Table 1:** Aircraft campaigns in the southeast Atlantic used for model evaluation during the biomass burning season

Campaign	Date range (Duration)	Instruments*	Aerodynamic Diameter (μm)	Altitude from surface (km)	Primary Reference
CLARIFY	7th August–4th September 2017 (99h)	C-ToF-AMS	0.05 to 0.60	0 to 8	Haywood et al., 2021
ORACLES	16th August–6th September 2017 (112h)	HR-ToF-AMS	0.07 and 0.70	0 to 7	Redemann et al., 2021

167   *Compact Time-of-Flight (C-ToF), High Resolution Time-of-Flight (HR-ToF), Aerosol Mass Spectrometer (AMS)

168   **3.1 Model Evaluation**

169   **3.1.1 Seasonal variation of AOD**

170   The spatial distribution of seasonal mean AOD from GEOS-Chem for the year 2017 is presented in Fig. 3. Three

171   distinct seasonal periods reflect dominant atmospheric and oceanic processes. These include the high DMS emission

172   period in the SEA, during the months of January, February, November, and December (JFND); the peak biomass

173   burning season in southern Africa, spanning from July to October (JASO); and the transitional season, encompassing

174   March, April, May, and June (MAMJ).
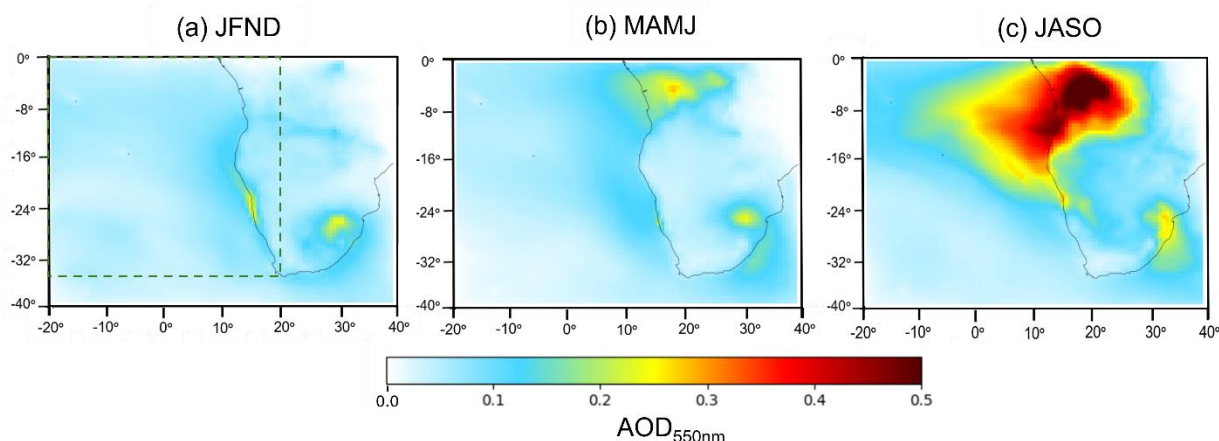
175

176   **Figure 3:** Spatial distribution of seasonal mean modeled AOD at 550 nm for 2017. Seasons are as follows: (a) the peak DMS

177   emission period (JFND), (b) the transitional period (MAMJ), and (c) the peak biomass burning period (JASO). The sub-domain

178   (0–35° S, 20° E–20° W) is highlighted with a green dotted rectangle in panel (a) for reference.

179   The simulated DMS emissions, based on Lana climatology (2011), indicates that emissions in the BUS region peak

180   in January, leading to elevated concentrations of sulfate aerosols. This increased sulfate (~20%), combined with dust

181   (59%) emissions from the Namib desert, contributes to an AOD hotspot as depicted in Fig. 3a on the southwestern

182   coast. In the JASO period (Fig. 3c), modeled AOD increases due to biomass burning aerosols, originating from

183   savannah fires in Central and southern Africa and transported westward towards the SEA region by the southern

184   African easterly jet (Adebiyi and Zuidema, 2016). The spatial distribution of mean transitional period AOD (Fig. 3b)

185   features hotspots in Congo and Angola which coincide with the onset of biomass burning in Central Africa.

186   Additionally, a year-round AOD hotspot is observed in northeastern South Africa (Gauteng province; Fig. 3), which

187   is associated with elevated aerosol concentrations due to industrial and mining activities, as well as domestic fuel

188   burning (Arowosegbe et al. 2021; Zhang et al. 2021).

189

190
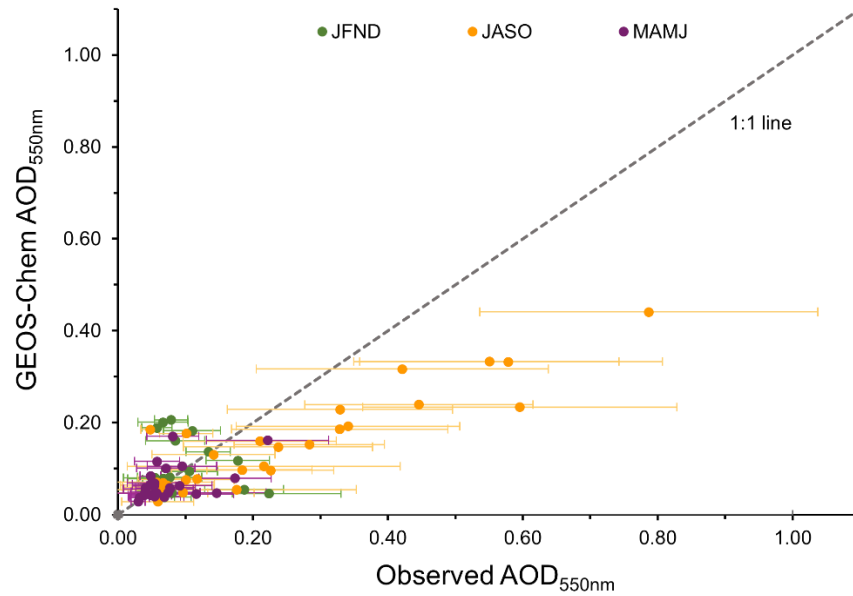
Figure 4: Modeled AOD_{550nm} (Y-axis) with respect to AERONET AOD_{550nm} (X-axis). Each data point represents the monthly mean values for each station color-coded by season (green- DMS period, yellow - biomass burning period, purple- transitional period). Error bars indicate the standard deviation of the AERONET AOD_{550nm} values, and the dotted line depicts the 1:1 relationship.

Figure 4 shows the correlation of monthly average AERONET and GEOS-Chem AOD across the nine selected sites (see Sect. 2.1 and Fig. 1), with the three seasonal periods distinguished by color: green for peak DMS emission season (JFND), yellow for biomass burning season (JASO), and purple for the transition period (MAMJ). Each data point corresponds to the monthly mean AOD values at distinct AERONET sites. The error bars in Fig. 4 represent the ± 1 standard deviation in monthly AOD measurements at these sites, with higher deviations observed during the biomass burning months (up to ± 0.25 at Namibe site). The comparison of monthly mean AOD across individual sites (see Table A2 in the Appendix) shows that, with the exception of Ascension Island, Gobabeb, and Upington, the mean AOD at the remaining sites during the biomass burning season (JASO) is atleast one standard deviation higher than the mean AOD in other seasons (JFND & MAMJ).

Table 2 compiles the performance of monthly mean GEOS-Chem AOD with respect to AERONET AOD by season. JASO exhibits the strongest correlation ($R = 0.901$), which is statistically significant ($p < 0.05$). The transitional period (MAMJ) shows a moderate correlation ($R = 0.48$) with a normalized mean bias (NMB) of 4.5%. Negligible negative correlation coefficient ($R = -0.058$) with a positive bias (29.8%) is seen during the summer period (JFND), predominantly due to anomalies at two sites. This period witnesses a considerable underestimation of AOD at Ascension Island, alongside an overestimation of dust aerosol at Gobabeb. Excluding these two sites, improves the model's correlation to 0.67 ($p = 0.55$) and reduces the NMB to 4.7%. This underestimate of AOD at Ascension Island (Fig. A1 in the Appendix) during summer (JFND) suggests potential model limitations in accurately simulating natural aerosol emissions such as sea salt and marine biogenic emissions. Meanwhile, the AOD discrepancy at Ascension

214 Island in the biomass burning season, may be due to the underestimate of transatlantic transport of light-absorbing
215 carbon aerosols (Das et al., 2017) and deviations in its spatial distribution from typical zonal patterns over the Atlantic
216 (Adebiyi et al., 2023). The sources of these model biases are discussed in further detail in Section 3.1.2.

217 **Table 2:** Statistical parameters of monthly mean modeled AOD with respect to observed AOD at the AERONET sites by season

Time period	Number of observations	Correlation coefficient (R)	Normalized mean bias (NMB) (%)	Root-mean square error (RMSE)
JFND	20	-0.058 (p = 0.62)	29.8	0.079
MAMJ	26	0.48 (p = 0.59)	4.5	0.043
JASO	28	0.901 (p = 0.044)	-18.6	0.15

218 We evaluate the relative aerosol speciation simulated at Ascension Island against monthly mean ACSM observations
219 during the LASIC campaign (see Sect. 2.2) available for January–November 2017 (Fig. A2 in the Appendix). The
220 seasonality of the relative contributions of organic aerosols and sulfate are consistent between the model and
221 observations. However, the model underestimates the relative contribution of sulfate during most months, while
222 generally overestimating the proportion of organics. An increase in the transport of biomass burning organic aerosols
223 would further worsen the model underestimate of sulfate. A slight overestimate in the modeled relative contribution
224 of sulfate is observed in February, and November, when simulated DMS emissions in the region are high (Lana et al.,
225 2011), largely due to enhanced underestimations of organics and nitrates.

226 **3.1.2 Vertical profiles of aerosol composition**

227 Figure 5 depicts the mean vertical profiles of speciated aerosol mass concentrations observed during ORACLES and
228 CLARIFY aircraft campaigns in August–September 2017 (the biomass burning season), compared to GEOS-Chem
229 (see Sect. 2.2 and Table 1). The cloud top height in the SEA region generally falls between 0 to 2 km (Redemann et
230 al., 2021). Findings from Diamond et al. (2018) indicate that aerosols below clouds in this lower atmospheric layer
231 can also substantially impact cloud microphysics. At these altitudes (0–2 km), GEOS-Chem performs well against
232 AMS measurements of total aerosol mass, which includes sulfate, nitrate, ammonium and organics from these
233 campaigns, with an NMB between -3.5% (CLARIFY) to -7.5% (ORACLES). At mid-altitudes (2–4 km), the model
234 is biased low, with NMB values spanning -19% (ORACLES) to -57% (CLARIFY). However, the model demonstrates
235 a pronounced bias at higher altitudes (4–7 km), where NMB values drop to -92% (ORACLES) to -93.5% (CLARIFY),
236 underscoring challenges in accurately modeling aerosol concentrations at these elevations. These significant low
237 biases in aerosol concentrations at higher altitude likely contribute to the model's underestimation of AOD during the

238   biomass burning period (see Section 3.1.1). This underestimation may also be affected by the model's bulk aerosol

239   scheme, which inadequately captures the optical properties of aerosols and is compounded by a low relative humidity

240   bias (Zhai et al., 2021). The bulk scheme also assumes all aerosols are externally mixed, which contrasts with the

241   variable degree of particle mixing states in the atmosphere (Yu et al., 2012; Dang et al., 2022). Moreover, studies like

242   Hodzic et al. (2020) using NASA ATom aircraft data indicate that GEOS-Chem substantially underestimates oxidation

243   levels of organic aerosols in remote areas, which could affect estimates of their burden and optical properties. Pai et

244   al. (2020) further suggests that the model underestimation of organic aerosol loading at mid-tropospheric heights is

245   linked to the surface injection treatment of fire emissions in GFED4.1s. Recent studies by Wizenberg et al. (2023) and

246   Marvin et al. (2024) concur that fire injection scheme is a critical source of model uncertainty, emphasizing the

247   potential importance of accurate fire injection modeling in the free troposphere. Nonetheless, our study focuses on

248   aerosol composition within cloud-relevant altitudes to improve our understanding of aerosol-cloud interactions and

249   their climate implications. The observed vertical distribution of aerosol mass concentrations (left panels of Fig. 5),

250   indicates that 18% and 36% of the aerosol mass for the ORACLES and CLARIFY campaigns, respectively, is located

251   below 2 km, within columns extending up to flight altitudes of 7 km and 8 km. However, the model simulates elevated

252   aerosol mass at these lower altitudes, 24% and 50% of the column for ORACLES and CLARIFY, respectively.
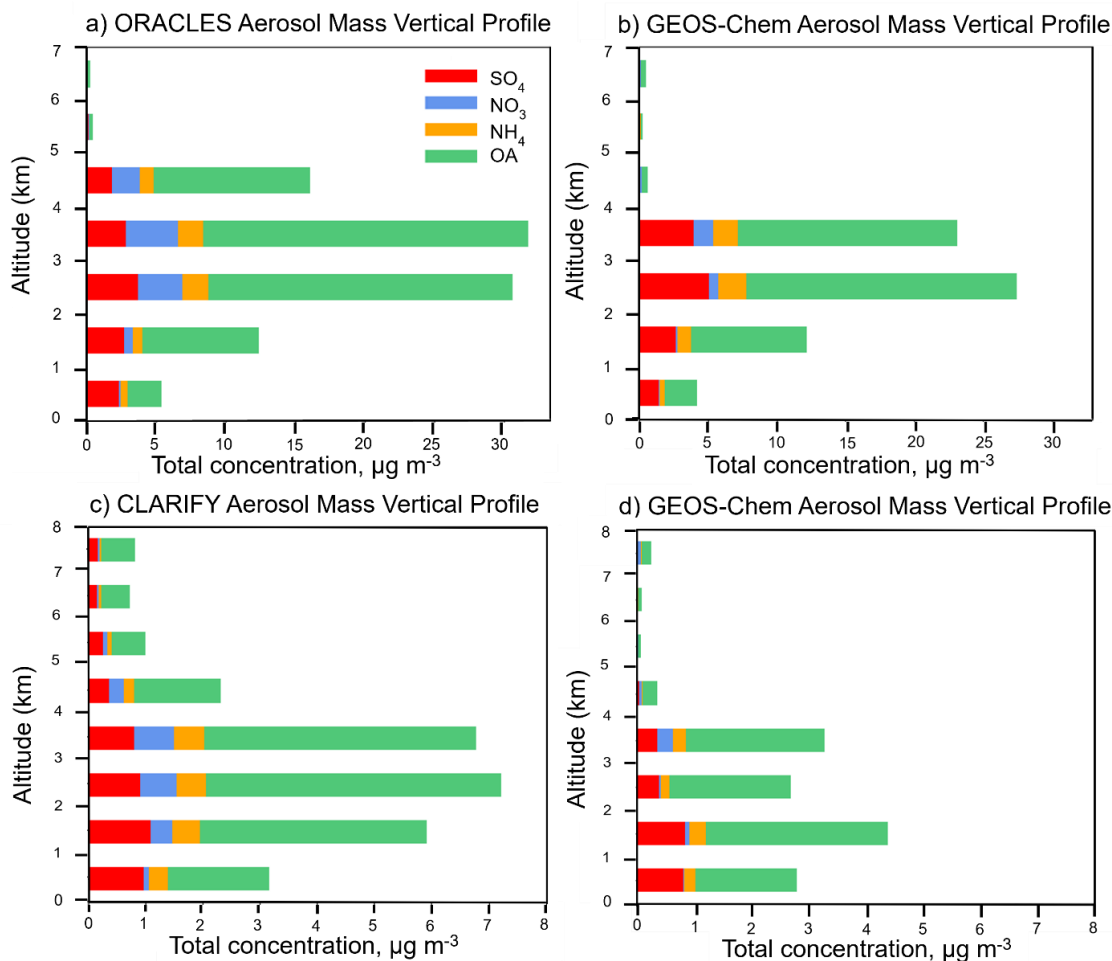
253

254 **Figure 5:** Average vertical profiles of simulated and observed aerosol mass during August–September 2017 (peak biomass burning
255 season) from aircraft campaigns. The left column presents the vertical distribution of aerosols observed during the ORACLES
256 flight campaign (panel a) and the CLARIFY flight campaign (panel c) at STP (see Sect. 2.3). The right column displays the GEOS-
257 Chem model simulations along the respective flight tracks of each campaign (panels b and d). All data are averaged over 1 km
258 vertical bins.

259 At altitudes where clouds persist in the domain (0 to 2 km), sulfate and organic aerosols are the dominant aerosol
260 types. Here, the model effectively captures the mass concentration of organic aerosols, with an NMB ranging from -
261 0.40% for ORACLES to -14% for CLARIFY. However, it underestimates sulfate aerosol concentrations by 19% at
262 cloud altitudes for both campaigns. For other aerosol types and altitudes, the model consistently underestimates
263 concentrations, except for sulfate and ammonium aerosols between 2 to 4 km during the ORACLES campaign, which
264 the model overestimates by 40% and 4.6%, respectively. The model captures the total aerosol mass from 0 through 7
265 km for sulfate and ammonium aerosols during the ORACLES campaign, with only minimal underestimations of 1.5%
266 and 0.7%, respectively. This indicates a potential discrepancy in the vertical distribution of these aerosols rather than
267 in total mass.

268 **3.2 Seasonal variation in aerosol composition and sources at cloud altitudes**

269
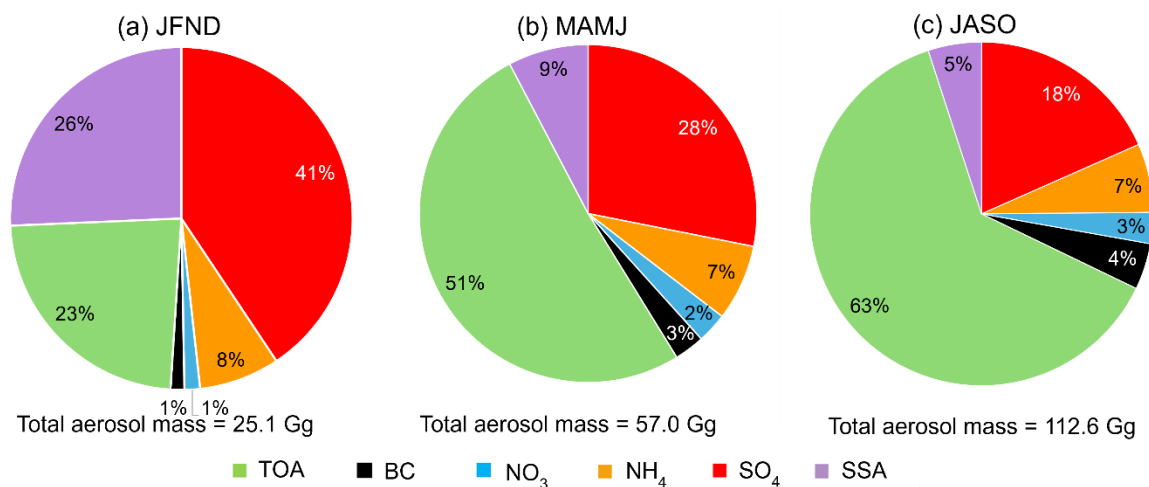
270 **Figure 6:** Simulated mean fractional aerosol composition at cloud heights (0 –2 km) over the ocean in the stratocumulus sub-
271 domain (0–35° S, 20° E–20° W) by season: (a) JFND, (b) MAMJ, and (c) JASO. Here SO_4, NH_4, NO_3, BC, TOA, SSA represent
272 sulfate, ammonium, nitrate, black carbon, total organic aerosol and accumulation-mode sea salt aerosols, respectively.

273 Figure 6 presents the simulated seasonal mean aerosol fractional composition within cloud-relevant altitudes (0-2 km),
274 averaged over the ocean only across the subdomain (0–35° S, 20° E – 20° W) (see the map shown in Fig. 7). This area
275 is strategically selected to coincide with the persistent Sc cloud deck and enhance our analysis of aerosol-cloud
276 interactions. Organic aerosols, an indicator of biomass burning, predominate during both the biomass burning (JASO)
277 and transitional (MAMJ) periods. In contrast, sulfate aerosols dominate during austral summer, likely influenced by
278 the high primary production from coastal upwelling that leads to DMS emissions. We investigate the model

279   representation of sulfate and these processes further in subsequent sections. An increase in the accumulation-mode

280   sea-salt aerosols (radius 0.01–0.5 μm) contribution (total mass of 6.7 Gg) is observed in summer (Fig. 6a) as well,

281   compared to other seasons (5.2 Gg during MAMJ and 5.8 Gg during JASO), owing to the peak wind speeds in the

282   southern Benguela region in this season (Hutchings et al., 2009). Black carbon, ammonium, and nitrate aerosols make

283   minor   contributions   to   simulated   aerosol   mass   at   cloud   height   throughout   the   year.
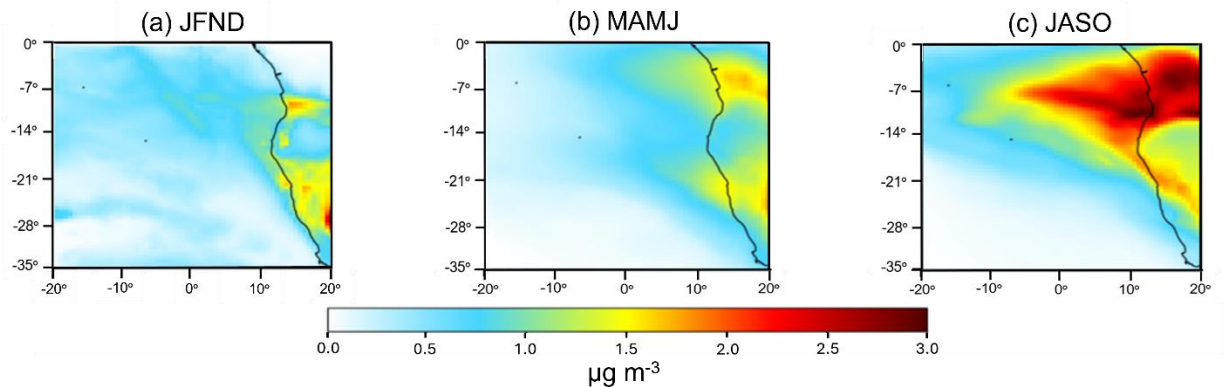
284

285   **Figure 7:** Spatial distribution of simulated mean sulfate aerosol concentrations averaged over cloud altitudes (0–2 km) in the sub-

286   domain (0–35° S, 20° E–20° W) by season in 2017: (a) peak DMS emission season (JFND), (b) transitional phase (MAMJ), and

287   (c) biomass burning season (JASO).

3.2.1 Drivers of sulfate aerosol and importance of marine precursor emissions

289   Sulfate aerosols are the most or 2nd most important aerosol component in cloud heights over the SEA (Fig. 6). We

290   examine the sources of sulfur emissions within the model in Figure 8. Within the broader domain (0–40° S, 40° E–

291   20° W), anthropogenic activities are the largest source of sulfur emissions throughout the year (Fig. 8). However, the

292   model default CEDS inventory (Hoesly et al., 2018) fails to capture the seasonality of these emissions due to absence

293   of regional inventories and reliance on the global datasets such as the International Energy Agency (IEA) energy

294   statistics. The anthropogenic emissions are followed by DMS emissions from the ocean, which become more

295   pronounced during the austral summer, peaking in January. Additionally, biomass burning contributes to SO$_2$

296   emissions seasonally, becoming the 3rd most important source of total sulfur emissions during July - September (Fig.

297   8). In contrast, sulfur contributions from volcanic, shipping, and aircraft emissions remain minimal and constant year-

298   round, reflecting assumptions of static fuel burned and emission levels across inventories.
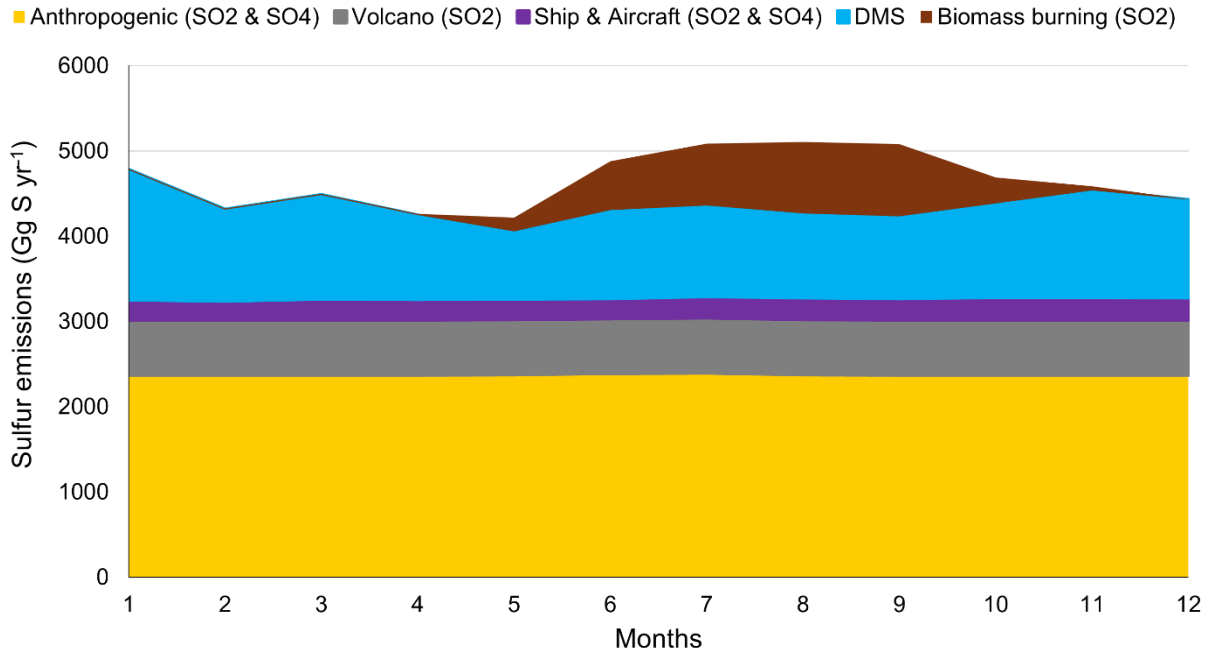
Figure 8: Stacked area chart of monthly total sulfur emissions by source for 2017 across the study domain (0–40° S, 40° E–20° W) in gigagrams of sulfur per year (Gg S yr^{-1}). Sources are indicated by color and encompass anthropogenic activities, volcanic activity, ship and aircraft emissions, biomass burning and natural emissions of dimethyl sulfide (DMS).

To improve understanding of the processes driving sulfate aerosol concentrations in the region, we examine its simulated spatial distribution averaged by season over the cloud height (0–2 km) in Fig. 7. Elevated concentrations of DMS, resulting from higher rates of primary production (Lana et al., 2011; Galí et al., 2018), lead to an increase in sulfate concentrations along the coastline of the Benguela region and the inner shelf of Namibia during JNFD (Fig. 7a), aligning with the AOD hotspot observed in Fig. 3a. This is consistent with the simulated dominance of sulfate aerosols at cloud-relevant altitudes during JFND (Fig. 6a). During the biomass burning months (JASO), while their relative contribution decreases (Fig. 6c), sulfate aerosols display a pronounced increase in absolute concentration (Fig. 7c) as a consequence of savanna fire emissions from southwestern Africa (van der Werf et al., 2010; Das et al., 2017). As outlined in the AOD evaluation (Sect. 3.1.1), the model underestimates the transport of emissions to remote sites (Fig A1), resulting in a steep gradient in sulfate concentrations from the eastern landmass towards the western open ocean.

To quantitatively estimate the contribution of marine precursor emissions to sulfate aerosols, we compare the sulfate mass between the standard and marine emissions only sensitivity simulations (Sect. 2.1). Figure 9 shows seasonally averaged vertical profiles over the ocean region of the Sc sub-domain (0°–35° S, 20° E–20° W). The figure presents the marine-only sulfate mass and the total sulfate mass from the standard simulation (left panels), and the ratio of marine sulfate to total sulfate (right panels). Vertical profiles were computed by summing the sulfate mass within each grid box, scaled by the grid box ocean fraction, across latitude and longitude within each vertical layer of the model, and then averaged temporally across each season.

321
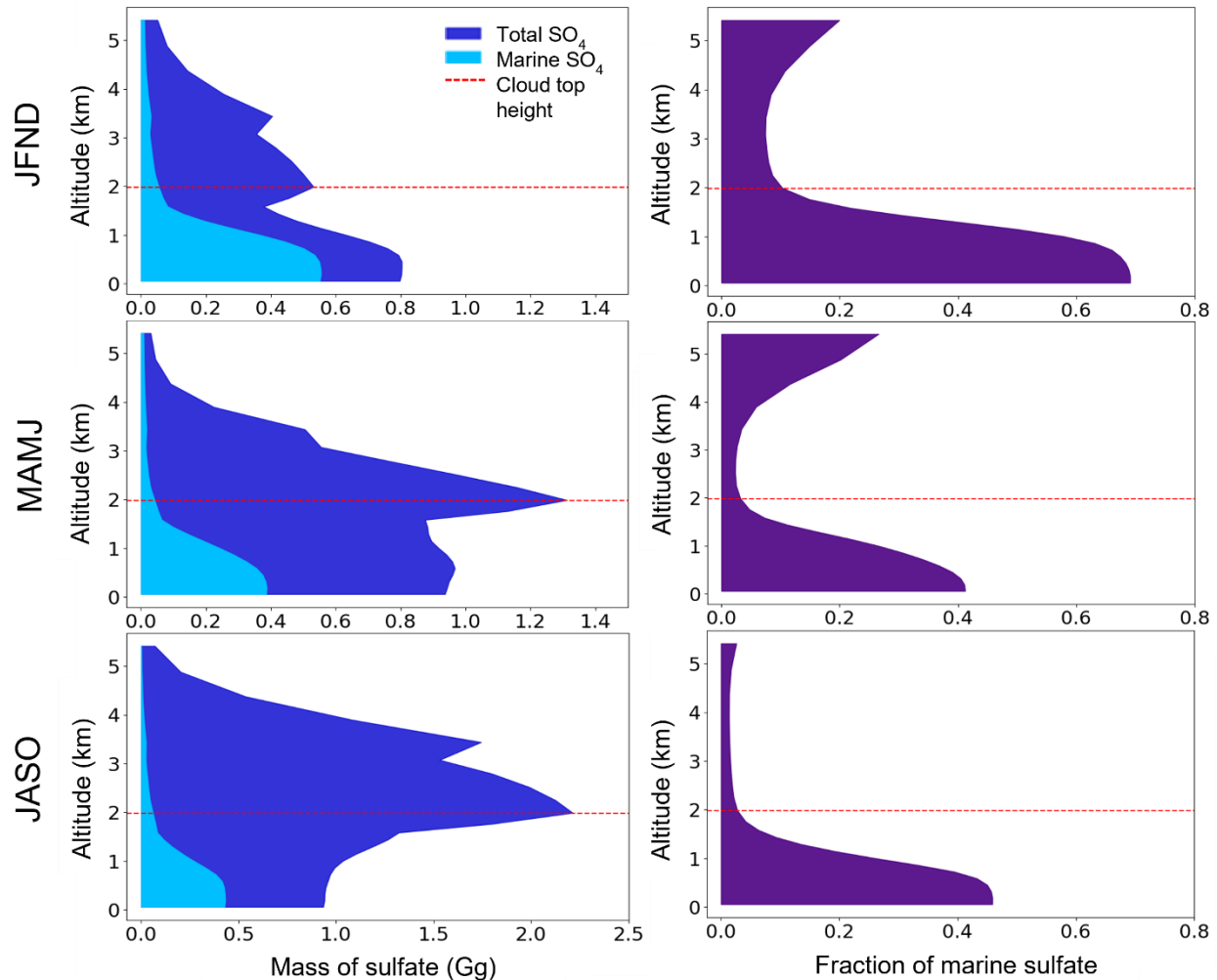
Figure 9: Simulated vertical profiles of sulfate aerosol mass over oceanic regions within the sub-domain (0°–35° S, 20° E–20° W) by season. The left panel shows the mass of total and marine sulfate aerosols, and the right panel indicates the sulfate fraction from marine sources. The top row corresponds to the peak dimethyl sulfide (DMS) emission period (JFND); the middle row to the transitional period (MAMJ); and the bottom row to the peak biomass burning period (JASO) (note: the bottom left panel displays a higher x-axis scale). The upper red dashed line denotes the typical maximum cloud top height (Redemann et al., 2021).

Our analysis highlights the substantial influence of marine sulfur sources on sulfate during JFND, as evidenced in the top left panel of Fig. 9. During this period the proportion of marine sulfate reaches up to 69.1% within-cloud (from surface to 2 km). The contribution of marine sulfate within the cloud in the subsequent periods is reduced (ranging between 2.7–45.9%; Fig. 9). We find that marine-sourced sulfate mass remains fairly consistent throughout the year (Fig. 9, left panels), with variations in the marine sulfate fraction (Fig. 9, right panels) mainly due to changes in land-based sulfate sources. Total sulfate mass during seasons influenced by biomass burning (MAMJ and JASO) peaks at 2 km, with greater mass above 2 km during peak biomass burning (JASO) in contrast to JFND where mass peaks within clouds (0–2 km).

335   Table 3 summarizes the monthly mean percent contribution of marine sulfate averaged across cloud altitudes (0–2
336   km). The annual average total sulfate mass and marine sulfate mass is 16.2 Gg and 3.5 Gg, respectively. The within-
337   cloud marine sulfate contribution peaks in January (57.7%) and is smallest in September (10.3%). Thus, our analysis
338   suggests that DMS emissions influence sulfate aerosol formation and their interactions with clouds in the region
339   throughout most of the year, excepting only the peak biomass burning season. This emphasizes that constraining
340   marine sulfur sources and chemistry both in chemical transport and climate models may improve representation of
341   aerosol-climate dynamics in the SEA region. Limited available observations suggest the model is biased low in AOD
342   throughout most of the year (Sect. 3.1.1), and underestimates sulfate aerosol concentrations in August and September
343   at cloud altitudes (Sect. 3.1.2, Fig. 5). We explore related uncertainties and their implications in the following
344   sections.

345   **Table 3:** Seasonal variation of percentage of monthly mean percent contribution of marine sulfate within cloud height.

Month	Percentage of marine sulfate
January	57.7
February	54.8
March	25.3
April	26.6
May	15.3
June	15.0
July	14.8
August	14.7
September	10.3
October	22.4
November	39.1
December	44.3

346

347 **3.3 Uncertainties**

348 **3.3.1 Assessing variations in DMS emission rates and oxidation mechanism on sulfate aerosol formation**

349 The Benguela region has substantial uncertainties in DMS concentrations in surface seawater (Asher et al., 2011;
350 Tortell et al., 2011) and the corresponding emission fluxes owing to the limited availability of biogenic sulfur
351 measurements. To investigate the sensitivity of DMS emission fluxes to changes in surface seawater DMS
352 concentrations, we conducted two simulations with DMS concentrations from Lana et al. (2011) and Galí et al. (2018)
353 (see Sect. 2.1). The standard results presented thus far were conducted using the Lana dataset.

354 In the southern Benguela, south of approximately 27° S, marked upwelling during the austral summer (Shannon and
355 Nelson, 1996; Hutchings et al., 2009) promotes phytoplankton growth and elevates DMS emissions. Figure 10
356 indicates that the Lana dataset aligns with this phenomenon, displaying peak DMS emission fluxes over the Sc sub-
357 domain in January. However, it lacks clear seasonality for the remaining months. In contrast, satellite-based DMS
358 estimates from Galí show pronounced emissions throughout the austral summer (JFND), as shown in Fig. 10. Both
359 datasets concur in magnitude for January and February, a period with better data coverage in the Lana et al. (2011)
360 climatological data set over the domain. However, the Lana dataset DMS emissions are up to 38% less during
361 December, while 51% higher in July relative to the Galí dataset. This suggests the marine contribution to sulfate in
362 our standard simulation using the Lana dataset may be underestimated from October through December
363 (encompassing two months of the peak DMS season) and overestimated from March through August (Fig. 10).
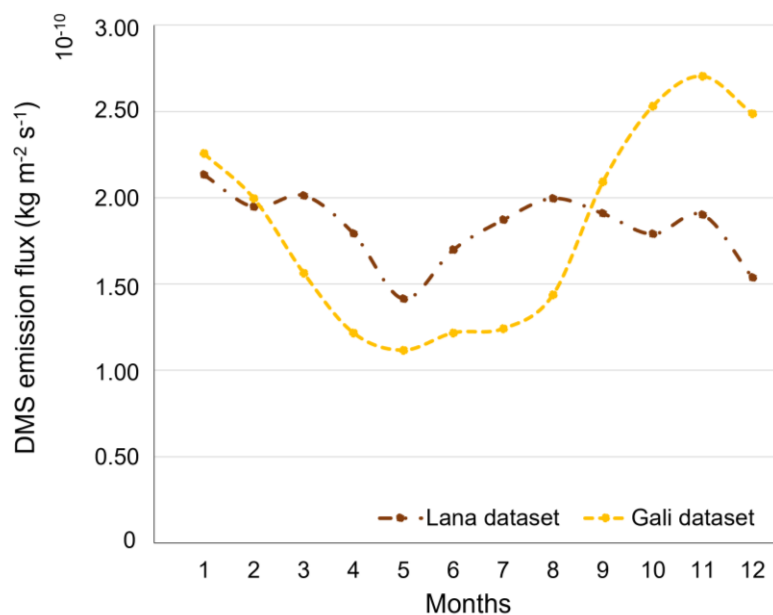
364

365 **Figure 10:** Monthly DMS emissions over the stratocumulus sub-domain (0–35° S, 20° E–20° W) using two distinct datasets for
366 surface seawater DMS concentrations. The brown dashed line presents emissions calculated using Lana et al. (2011) climatology,

367 which compiles data across 1972-2009 from multiple sources. In contrast, the yellow dashed line depicts emissions based on
368 satellite-derived estimates of surface seawater DMS concentrations (Galí et al., 2018).

369 The ongoing discovery of complexities within DMS oxidation mechanisms, along with the incomplete incorporation
370 of these mechanisms into atmospheric chemistry models, further contributes to uncertainties in predicting the impact
371 of DMS emissions on aerosols and climate (Faloona, 2009; Quinn and Bates, 2011; Carslaw et al., 2013). Chen et al.
372 (2018) highlighted the impacts of changes to DMS chemistry in the GEOS-Chem model, integrating a series of
373 multiphase sulfur oxidation mechanisms and two DMS intermediates, which led to a decrease in the global DMS
374 burden, thereby decreasing SO_2 and sulfate levels. On the other hand, Novak et al. (2021) found that the cloud uptake
375 of hydroperoxymethyl thioformate (HPMTF), a newly identified oxidation product of DMS (Wu et al., 2015; Veres
376 et al., 2020), lowers near-surface SO_2 concentration while elevating sulfate concentration in the model. Most recently,
377 Tashmim et al. (2024) implemented an advanced DMS oxidation mechanism in GEOS-Chem that incorporates the
378 latest developments in DMS chemistry, including those previously mentioned, which led to a lower SO_2 mixing ratio
379 (~70%) and a higher SO_4 mixing ratio (~35%) over the SEA during austral summer. Thus, an improved representation
380 of DMS emissions and oxidation chemistry in the model could enhance the sulfate aerosol estimations during the peak
381 DMS season. This refinement may address model underestimates of aerosol concentrations during this period (Sect.
382 3.1.1).

383 **3.3.2 Exploring the impact of marine organic aerosol emissions on organic aerosol concentrations**

384 Beyond marine sulfate and sea-salt aerosols, organic matter also makes a significant contribution to marine aerosol
385 mass (Middlebrook et al., 1998; Oppo et al., 1999; Russell et al., 2010). Notably, substantial concentrations of organic
386 carbon aerosols have been observed in marine regions, particularly during periods of intense biological activity
387 (O'Dowd et al., 2004). These aerosols can also increase CCN, affecting cloud properties and radiative balance (Arnold
388 et al., 2009; Gantt and Meskhidze, 2013). However, the standard GEOS-Chem model does not account for these
389 marine organic aerosol emissions. Here, we analyzed the impact of marine POA on cloud-altitude aerosols over the
390 SEA by incorporating marine POA emissions based on satellite-derived chlorophyll-a concentrations (Gantt et al.,
391 2015; See Sect. 2.1) in the model.
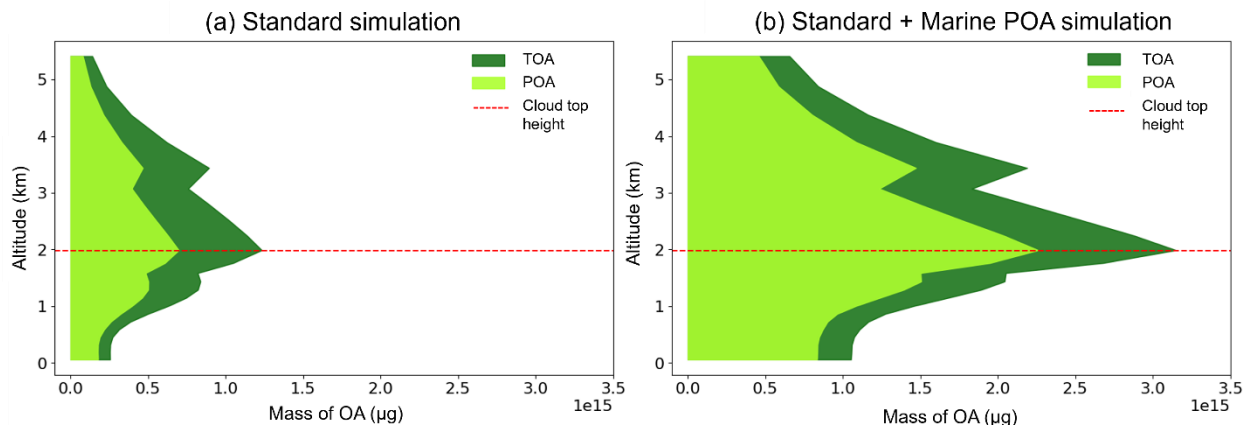
392

393 **Figure 11:** Vertical distribution of organic aerosol mass during November 2017, the month of maximum discrepancy between the
394 standard and MPOA simulations, over the Sc sub-domain (0–35° S, 20° E–20° W). Left: mass profile for total organic aerosols
395 (TOA) and primary organic aerosols (POA) under standard simulation conditions (Std); right: when marine primary organic aerosol
396 (MPOA) emissions are included (Std + MPOA). The red dashed line indicates the typical maximum cloud top height.

397 We find that the inclusion of MPOA emissions consistently resulted in higher organic aerosol mass, with the greatest
398 increase in November. Figure 11 shows the vertical distribution of total organic aerosols (TOA) mass and POA mass
399 (including MPOA and other POA sources) with and without MPOA emissions during this month. Similar to our earlier
400 vertical profile analysis (refer to Sect. 3.2.2), we find that the maximum organic aerosol mass occurred at the highest
401 cloud top height (2 km). The Standard + MPOA simulated peak total organic aerosol mass was approximately three
402 times higher than that in the Standard simulation, highlighting the potential contribution of marine sources to total
403 organic aerosol mass concentrations. However, during the biomass burning season, the sensitivity simulation showed
404 only a minimal increase, indicating that it does not adequately address the model's underestimation (refer to Fig. 5).
405 Gantt et al. (2015) demonstrated that including MPOA emissions in GEOS-Chem reduced the normalized mean bias
406 (NMB) of surface organic aerosol concentrations at coastal sites by 67%. Additionally, Pai et al. (2020) noted that
407 without a marine POA source, the model fails to accurately reproduce lower-tropospheric concentrations over oceans,
408 although the marine POA scheme might be biased high. Despite the limitations of a chlorophyll-based
409 parameterization like the one used here in providing mechanistic understanding of the seasonal and geographical
410 variability of organic matter emissions from sea spray (Burrows et al., 2022), our findings suggest that MPOA may
411 play a role in aerosol-cloud interactions outside of the biomass burning season, in addition to marine-derived sulfate
412 from DMS (Sect. 3.2).

413 **3.3.3 Impacts of uncertainties in biomass burning emissions of SO_2**

414 To assess the impact of uncertainty in biomass burning emissions of SO_2 on the relative contribution of marine vs.
415 land sources to aerosol, we performed a sensitivity analysis using two alternative inventories, QFED and GFAS (see
416 Sect. 2.1 and Fig. A3). The standard simulations, as detailed in Sect. 2.3, use the default biomass burning inventory
417 in GEOS-Chem, GFED. The GFAS inventory SO_2 and CO emissions over the domain are constant in time, aligning
418 with QFED during the non-biomass burning months (Fig. A3). We find that CO emissions from GFED and QFED
419 align closely; however, there is a notable difference in SO_2 emissions between the two inventories (Fig. A3). These
420 discrepancies likely originate from variations in SO_2 emission factors employed by each inventory. In July, which
421 exhibits the largest difference between the two inventories, peak SO_2 emissions in QFED are almost five-fold higher
422 than those in GFED. This discrepancy leads to a 25% increase in sulfate aerosol concentrations at cloud altitudes
423 relative to the standard results using GFED (not shown). Consequently, the contribution of marine sulfate to total
424 sulfate (see Sect. 3.2.1) may further decrease during the peak biomass burning season if QFED is used, highlighting
425 the sensitivity of aerosol source attributions to the selected biomass burning inventory.

426 **4 Implications**

427 In this study, monthly marine sulfate constitutes between 10.3% and 57.7% of total sulfate within the cloud height,
428 peaking during the high DMS emission period. However, the default Lana et al. (2011) climatology largely
429 underestimates DMS emissions during the austral summer (November and December) by up to 38%, compared to the
430 satellite-derived estimates from Galí et al. (2018). Moreover, improvement of DMS chemistry in the model by
431 incorporating new oxidation mechanisms and intermediate products could shift the balance towards increased sulfate
432 aerosol production (with Tashmim et al., 2024 suggesting an increase of up to 35% over the SEA). Marine primary
433 organic aerosol emissions may also contribute substantially to the organic aerosol mass during the peak primary
434 production period (JNFD), highlighting the importance of marine contributions to overall aerosol concentrations.
435 Meanwhile, discrepancies in SO_2 emissions from biomass burning can increase sulfate aerosol from biomass burning
436 by up to 25%. These changes would improve the model underestimate of AOD relative to AERONET observations;
437 however, observations of aerosol composition outside of August-September are very limited and this is a large gap.
438 Our results suggest marine-sourced sulfate and organics significantly influence aerosol loading and composition in
439 the SEA, particularly during the non-biomass burning period. Accurately characterizing the seasonal dynamics of
440 aerosols within cloud heights is imperative for quantifying aerosol-cloud interactions and understanding the dynamics
441 of marine aerosols in the SEA region, where uncertainties in aerosol radiative forcing are most pronounced. This
442 understanding is essential for improving the reliability of climate models in areas critical to both regional and global
443 climate dynamics.

444 **5 Conclusion**

445 Aerosols over the southeast Atlantic strongly influence global climate dynamics due to the presence of persistent
446 stratocumulus clouds and large uncertainties in aerosol-cloud interactions. However, precisely representing these
447 interactions in global climate models remains challenging, in part due to sparse available observations, especially
448 outside of the biomass burning season. In this study, we employed the GEOS-Chem chemical transport model to
449 assess the aerosol composition at cloud-relevant altitudes (0–2 km) and identify the sensitivities to marine emissions
450 and chemistry in the southeast Atlantic. This analysis aims to enhance our understanding of the role of marine aerosols
451 and the associated uncertainties affecting aerosol-cloud interactions within this climate-sensitive region.

452 We performed nested grid simulations with a 0.5° x 0.625° horizontal resolution and evaluated the model against
453 ground-based and aircraft campaign observations throughout 2017. We analyzed results for three seasonal periods
454 with distinct dominant processes including (a) the high DMS emission season (JFND), (b) the peak biomass burning
455 season (JASO), and (c) the transitional season (MAMJ). Our analysis showed that simulated monthly average aerosol
456 optical depth (AOD) exhibits the strongest correlation (R = 0.901) with the AERONET AOD observations during the
457 JASO season. However, the model generally underestimates AOD throughout the year, except in the JFND period,
458 where an overestimate at Gobabeb site offset underestimations at other sites. Moreover, a comparison of aerosol
459 speciation measured at Ascension Island during the LASIC campaign indicates that the model consistently
460 underestimates sulfate aerosols. We further evaluated the simulated vertical profile of aerosol mass concentrations
461 and composition against measurements from the ORACLES and CLARIFY campaigns. These comparisons showed
462 that sulfate aerosols were underestimated by 19% at cloud-relevant altitudes of 0–2 km by both campaigns. The

463 underestimate of sulfate aerosols at lower altitudes (0-2 km), coupled with an underestimate of other aerosols at higher
464 altitudes (4-8 km), likely contributes to the overall low bias in modeled AOD. The misrepresentation of natural aerosol
465 emissions and transatlantic aerosol transport may be responsible for these underestimates. Nevertheless, discrepancies
466 increase with altitude, reflecting challenges in accurately modeling high-altitude aerosol concentrations.

467 Analysis of seasonal mean aerosol composition at cloud height showed that organic aerosols predominate during
468 JASO (63%) and MAMJ (51%), while sulfate aerosols are most prevalent (41%) during the austral summer (JFND).
469 Given the prominence of sulfate as a marine sourced aerosol in remote oceanic environments, we investigated the
470 processes influencing the sulfate aerosol concentrations in our domain. Throughout the year, anthropogenic sources
471 and oceanic DMS emissions are the primary atmospheric sulfur contributors. Spatial mapping across the sub-domain
472 (0–35° S, 20° E–20° W) showed high sulfate concentrations (up to $3\mu g\ m^{-3}$) at cloud height during the peak biomass
473 burning season (JASO), primarily from savannah fires in southern Africa. Despite this, sulfate aerosols only account
474 for 18% of the total aerosol mass in JASO.

475 Sulfate, primarily from marine sources, is the dominant aerosol at cloud-relevant altitudes during JFND in the model
476 (up to 69% marine contribution); however, significant uncertainties regarding the treatment of DMS persist that may
477 affect this finding. To assess the impact of these uncertainties on sulfate aerosols, we compared DMS emission fluxes
478 from Lana et al. (2011) climatological data, which has limited spatial and temporal coverage in our domain, with those
479 from Galí et al. (2018), which are based on satellite-based estimates of surface seawater DMS concentrations. We find
480 that, within our domain, the Lana dataset emissions estimates are 51% higher in July and 38% lower in December
481 compared to the Galí dataset. Moreover, improvement of DMS chemistry in the model by incorporating new oxidation
482 mechanisms and intermediate products could shift the balance towards increased sulfate aerosol production (with
483 Tashmim et al., 2024 suggesting an increase of up to 35% over the SEA). Additionally, emissions of marine primary
484 organic aerosols during the peak primary production period (JNFD) may substantially contribute to the mass of organic
485 aerosols which can also act as CCN. This emphasizes the critical role of marine sources in influencing aerosol
486 concentrations, even in oceanic regions impacted by large seasonal biomass burning. Variations in SO_2 emissions
487 from biomass burning could potentially increase sulfate aerosol concentrations at cloud altitudes by up to 25%.
488 Addressing these discrepancies is essential for improving the model's underestimation of AOD and aerosol
489 concentrations compared to observations.

490 This study highlights the importance of constraining marine emissions and their chemical transformations by
491 incorporating satellite-retrieved datasets and extending field campaign efforts during non-biomass burning periods.
492 Such initiatives are essential to accurately characterize seasonal aerosol dynamics at cloud heights and to improve our
493 understanding of aerosol-cloud interactions in regions with persistent low-altitude clouds. These advancements could
494 substantially minimize uncertainties in model estimates of radiative forcing and enhance the reliability of climate
495 model projections in the southeast Atlantic region.

496

497

Appendix A

Table A1: Configuration of sensitivity analysis simulations

Simulations	Resolution	Emission inventories (References)
Marine sulfur emissions only	0.5° x 0.625°	Standard model inventories (see Section 2.1 in the main text)
DMS emissions	4° x 5°	Climatological product for seawater DMS (Lana et al., 2011); Satellite-derived DMS estimates (Galí et al., 2018)
Biomass burning inventories	4° x 5°	Global Fire Emissions Database (van der Werf et al., 2017); Quick Fire Emissions Dataset (Darmenov & da Silva, 2013); Global Fire Assimilation System (Kaiser et al., 2012).
Marine primary organics	0.5° x 0.625°	Marine primary organic aerosol emission estimates from satellite-derived chlorophyll-a concentrations (Gantt et al., 2015)

500
501

502

503

504

505

506

507

508 **Table A2:** AERONET site information and the monthly average AOD$_{550}$ value (± 1 standard deviation) for three
509 distinct time periods per site are shown. An asterisk (first column) indicates that the mean AOD during the biomass
510 burning season (JASO) at these sites is more than 1 standard deviation higher than the mean AOD in other season(s)
511 (JFND and MAMJ).

Site	Latitude (°)	Longitude (°)	Months of data availability for 2017	Monthly Average AOD$_{550nm}$ ± 1 SD (JFND)	Monthly Average AOD$_{550nm}$ ± 1 SD (MAMJ)	Monthly Average AOD$_{550nm}$ ± 1 SD (JASO)
Ascension Island	-7.976	-14.415	7	0.320 ± 0.061	0.256 ± 0.046	0.396 ± 0.078
Gobabeb	-23.562	15.041	12	0.268 ± 0.033	0.254 ± 0.032	0.399 ± 0.115
HESS*	-23.273	16.503	10	0.162 ± 0.024	0.211 ± 0.033	0.368 ± 0.108
Henties_Bay*	-22.095	14.26	3	0.166 ± 0.021	0.138 ± 0.021	0.380 ± 0.114
Lubango*	-14.958	13.445	9	0.120 ± 0.011	0.251 ± 0.011	0.534 ± 0.139
Namibe*	-15.159	12.178	8	0.279 ± 0.028	0.314 ± 0.029	0.689 ± 0.192
Simonstown_IMT*	-34.193	18.446	7	0.246 ± 0.049	0.179 ± 0.018	N/A
Upington	-28.379	21.156	8	0.131 ± 0.019	0.193 ± 0.035	0.321 ± 0.115
Windport*	-19.366	15.483	10	0.249 ± 0.041	0.242 ± 0.037	0.514 ± 0.159

512
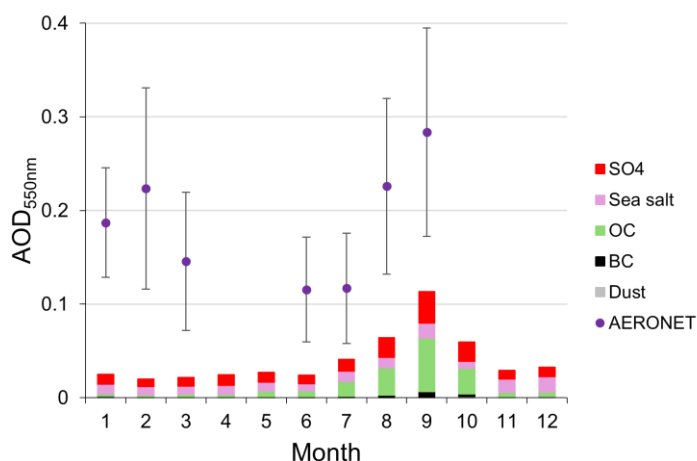
513

514 **Figure A1:** Comparative analysis of aerosol optical depth at 550 nm (AOD$_{550nm}$) for Ascension Island in 2017. The
515 purple dots present the measured mean monthly AOD values, with vertical error bars illustrating the range of AOD$_{550nm}$
516 measurements captured by the AERONET ground station. The stacked bars represent the GEOS-Chem model's

517   simulated AOD values, with each layer corresponding to the major aerosol components, such as sulfate (SO_4), sea

518   salt, organic carbon (OC), black carbon (BC), and dust, providing insight into the model's aerosol composition

519   representation.
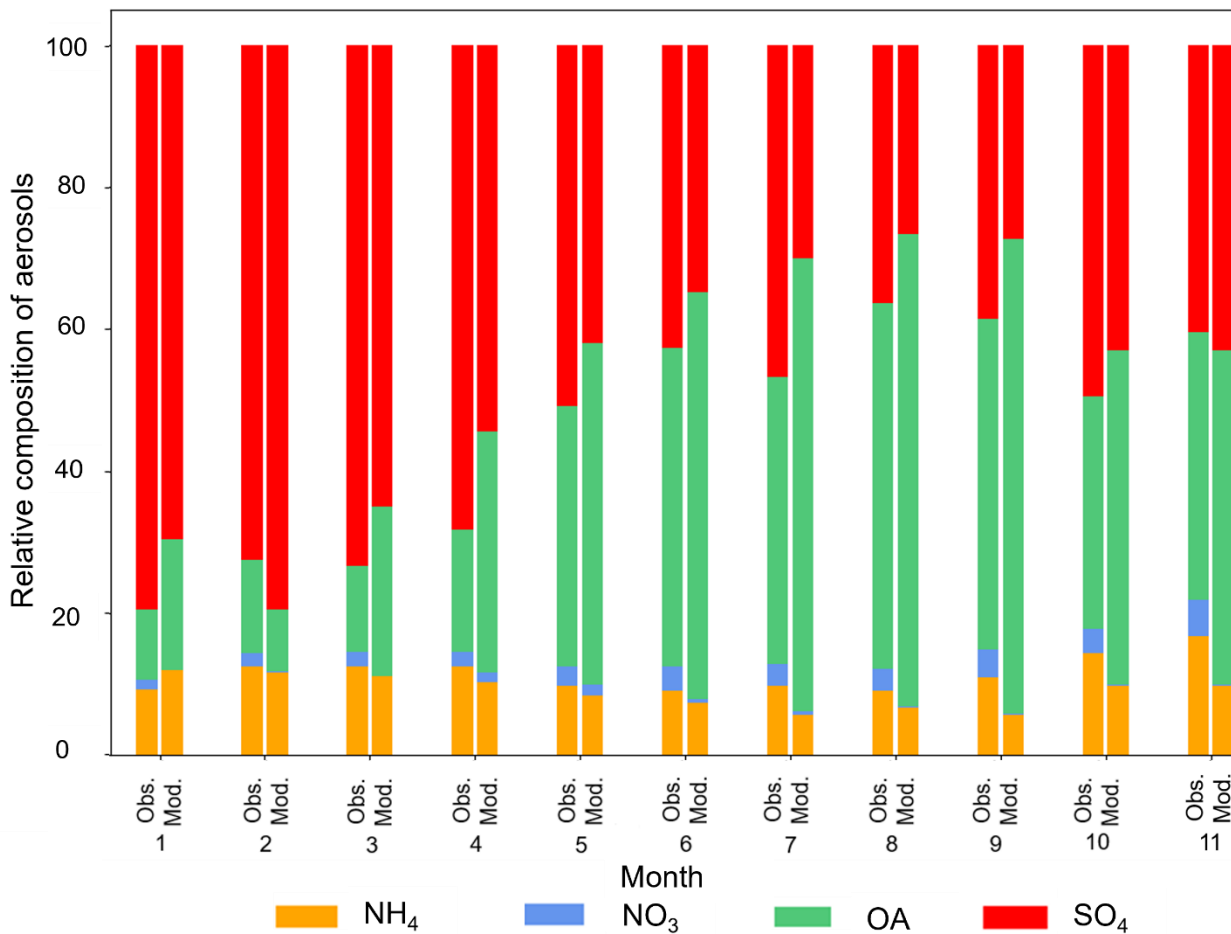
520

521   **Figure A2:** Comparative analysis of the relative aerosol composition at Ascension Island in 2017. The stacked bars

522   on the left depict observations of chemical composition taken during the LASIC campaign at the ARM facility on

523   Ascension Island, utilizing an aerosol chemical speciation monitor (ACSM) at 341 meters. The bars on the right

524   illustrate the GEOS-Chem simulated aerosol composition at the same coordinates. Each segment of the stack

525   represents different aerosol components: ammonium (NH_4), nitrates (NO_3), organic aerosols (OA), and sulfate (SO_4).

526

527

528

529

530

531
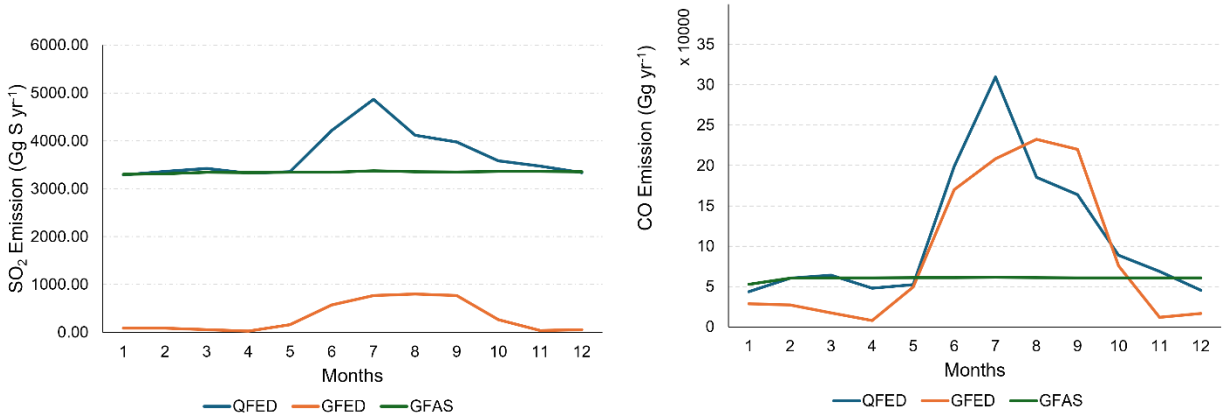
Figure A3: Comparison of biomass burning emissions across various inventories, namely GFED, QFED, and GFAS across the domain (0–40° S, 40° E–20° W). The panels depict the interannual variability of biomass burning emissions, with the left panel illustrating sulfur dioxide (SO₂) emissions, and the right panel displaying carbon monoxide (CO) emissions. Both GFED and QFED indicate similar emission trends; however, GFED exhibits lower SO₂ emission magnitudes compared to QFED. GFAS presents emission magnitudes similar to QFED during non-biomass burning period.

Code and data availability

The GEOS-Chem model used here is publicly available at https://zenodo.org/records/5748260. The ORACLES campaign data from 2017 are available at: https://doi.org/10.5067/Suborbital/ORACLES/P3/2017_V2 (last access January 26, 2024). The CLARIFY campaign data are available at https://catalogue.ceda.ac.uk/uuid/38ab7089781a4560b067dd6c20af3769 (last access February 12, 2024). The ACSM dataset from LASIC campaign is available at https://doi.org/10.5439/1763029 (last access September 10, 2024).

Author contributions

MH, HMH, and RMG designed the research. MH conducted the model simulations, analysis, and visualization, with expert advice from HMH. MH drafted the manuscript, which was then revised by all co-authors.

Competing interests

At least one of the (co-)authors is a member of the editorial board of Atmospheric Chemistry and Physics.

Acknowledgements

Mashiat Hossain and Hannah M. Horowitz gratefully acknowledge Michael Diamond for discussions on cloud-relevant altitudes over the southeast Atlantic region.

References

Adebiyi, A. A., and Zuidema, P.: The role of the southern African easterly jet in modifying the southeast Atlantic aerosol and cloud environments, Q. J. Roy., 142, https://doi.org/10.1002/qj.2765, 2016.

Adebiyi, A. A., Zuidema, P., and Abel, S. J.: The convolution of dynamics and moisture with the presence of shortwave absorbing aerosols over the southeast Atlantic, JCLI, 28, https://doi.org/10.1175/JCLI-D-14-00352.1, 2015.

Adebiyi, A. A., Akinsanola, A. A., and Ajoku, O. F.: The Misrepresentation of the Southern African Easterly Jet in Models and Its Implications for Aerosol, Clouds, and Precipitation Distributions, JCLI, 36, https://doi.org/10.1175/JCLI-D-23-0083.1, 2023.

Alexander, B., Park, R. J., Jacob, D. J., and Gong, S.: Transition metal-catalyzed oxidation of atmospheric sulfur: Global implications for the sulfur budget. J. Geophys. Res., 114, https://doi.org/10.1029/2008JD010486, 2009.

Andreae, M. O.: Ocean-atmosphere interactions in the global biogeochemical sulfur cycle, Mar. Chem., 30, https://doi.org/10.1016/0304-4203(90)90059-L, 1990.

Andreae, M. O., Elbert, W., and De Mora, S. J.: Biogenic sulfur emissions and aerosols over the tropical South Atlantic. 3. Atmospheric dimethylsulfide, aerosols and cloud condensation nuclei, J. Geophys. Res., 100, https://doi.org/10.1029/94jd02828, 1995.

Arnold, S. R., Spracklen, D. V., Williams, J., Yassaa, N., Sciare, J., Bonsang, B., Gros, V., Peeken, I., Lewis, A. C., Alvain, S., and Alvain, M.: Evaluation of the global oceanic isoprene source and its impacts on marine organic carbon aerosol, Atmos. Chem. Phys., 9, https://doi.org/10.5194/acp-9-1253-2009, 2009.

Arowosegbe, O. O., Röösli, M., Adebayo-Ojo, T. C., Dalvie, M. A., and de Hoogh, K.: Spatial and Temporal Variations in PM_{10} Concentrations between 2010–2017 in South Africa, Int. J. Environ. Res. Public Health, 18, 1-12, doi.org/10.1016/j.envpol.2022.119883, 2021.

Asher, E.C., Merzouk, A., and Tortell, P.D.: Fine-scale spatial and temporal variability of surface water dimethylsufide (DMS) concentrations and sea–air fluxes in the NE Subarctic Pacific, *Mar. Chem.*, *126*, 63-75, https://doi.org/10.1016/j.marchem.2011.03.009, 2011.

Barnes, I., Hjorth, J., and Mihalapoulos, N.: Dimethyl sulfide and dimethyl sulfoxide and their oxidation in the atmosphere, Chem. Rev., 106, https://doi.org/10.1021/cr020529, 2006.

Barrett, P. A., Abel, S. J., Coe, H., Crawford, I., Dobracki, A., Haywood, J., Howell, S., Jones, A., Langridge, J., McFarquhar, G. M., Nott, G. J., Price, H., Redemann, J., Shinozuka, Y., Szpek, K., Taylor, J. W., Wood, R., Wu, H., Zuidema, P., … Zhang, J.: Intercomparison of airborne and surface-based measurements during the CLARIFY, ORACLES and LASIC field experiments, Atmos. Meas. Tech., 15, 6329–6371. https://doi.org/10.5194/amt-15-6329-2022, 2022.

Bates, T. S., Lamb, B. K., Guenther, A., Dignon, J., and Stoiber, R. E.: Sulfur emissions to the atmosphere from natural sources, J. Atmos. Chem., 14, 1–4, https://doi.org/10.1007/BF00115242, 1992.

Brooks, S. D., and Thornton, D. C. O.: Marine aerosols and clouds, Ann. Rev. Mar. Sci., 10, https://doi.org/10.1146/annurev-marine-121916-063148, 2018.

Burkholder, J. B., Sander, S. P., Abbatt, J., Barker, J. R., Huie, R. E., Kolb, C. E., Kurylo, M. J., Orkin, V. L., Wilmouth, D. M., and Wine, P. H.: Chemical Kinetics and Photochemical Data for Use in Atmospheric Studies, Evaluation No. 18, JPL Publication 15-10, Jet Propulsion Laboratory, Pasadena, available at: http://jpldataeval.jpl.nasa.gov (last access: 10 May 2024), 2015.

Burrows, S. M., Easter, R. C., Liu, X., Ma, P. L., Wang, H., Elliott, S. M., Singh, B., Zhang, K., and Rasch, P. J.: OCEANFILMS (Organic Compounds from Ecosystems to Aerosols: Natural Films and Interfaces via Langmuir Molecular Surfactants) sea spray organic aerosol emissions - implementation in a global climate model and impacts on clouds, Atmos. Chem. Phys., 22, https://doi.org/10.5194/acp-22-5223-2022, 2022.

Carslaw, K. S., Lee, L. A., Reddington, C. L., Pringle, K. J., Rap, A., Forster, P. M., Mann, G. W., Spracklen, D. V., Woodhouse, M. T., Regayre, L. A., and Pierce, J. R.: Large contribution of natural aerosols to uncertainty in indirect forcing, Nature, 503, https://doi.org/10.1038/nature12674, 2013.

Chen, H., Ezell, M. J., Arquero, K. D., Varner, M. E., Dawson, M. L., Gerber, R. B., and Finlayson-Pitts, B. J.: New particle formation and growth from methanesulfonic acid, trimethylamine and water, Phys. Chem. Chem. Phys., 17, https://doi.org/10.1039/c5cp00838g , 2015.

Chen, Q., Sherwen, T., Evans, M., and Alexander, B.: DMS oxidation and sulfur aerosol formation in the marine troposphere: A focus on reactive halogen and multiphase chemistry, Atmos. Chem. Phys., 18, https://doi.org/10.5194/acp-18-13617-2018, 2018.

Chen, Y. C., Christensen, M. W., Stephens, G. L., and Seinfeld, J. H.: Satellite-based estimate of global aerosol-cloud radiative forcing by marine warm clouds, Nat. Geosci., 7, https://doi.org/10.1038/ngeo2214, 2014.

Chin, M., Jacob, D. J., Gardner, G. M., Foreman-Fowler, M. S., Spiro, P. A., and Savoie, D. L.: A global three-dimensional model of tropospheric sulfate, J. Geophys. Res., 101, https://doi.org/10.1029/96jd01221, 1996.

Croft, B., Martin, R. V., Moore, R. H., Ziemba, L. D., Crosbie, E. C., Liu, H., Russell, L. M., Saliba, G., Wisthaler, A., Müller, M., Schiller, A., Galí, M., Chang, R. Y. W., McDuffie, E. E., Bilsback, K. R., and Pierce, J. R.: Factors controlling marine aerosol size distributions and their climate effects over the northwest Atlantic Ocean region, Atmos. Chem. Phys., 21, https://doi.org/10.5194/acp-21-1889-2021, 2021.

Dang, C., Segal-Rozenhaimer, M., Che, H., Zhang, L., Formenti, P., Taylor, J., Dobracki, A., Purdue, S., Wong, P., Nenes, A., Sedlacek III, A., Coe, H., Redemann, J., Zuidema, P., Howell, S., and Haywood, J.: Biomass burning and marine aerosol processing over the southeast Atlantic Ocean: a TEM single-particle analysis, Atmos. Chem. Phys., 22, 9389-9412, 10.5194/acp-22-9389-2022, 2022 .

Darmenov, A., and da Silva, A. M.: The Quick Fire Emissions Dataset (QFED) - Documentation of versions 2.1, 2.2 and 2.4. NASA Tech. Rep. Ser. Glob. Model. Data Assim. NASA TM-2013-104606, 32, 1–183, 2013.

Das, S., Harshvardhan, H., Bian, H., Chin, M., Curci, G., Protonotariou, A. P., Mielonen, T., Zhang, K., Wang, H., and Liu, X.: Biomass burning aerosol transport and vertical distribution over the South African-Atlantic region, J. Geophys. Res., 122, https://doi.org/10.1002/2016JD026421, 2017.

Diamond, M. S., Dobracki, A., Freitag, S., Griswold, J. D. S., Heikkila, A., Howell, S. G., Kacarab, M. E., Podolske, J. R., Saide, P. E., and Wood, R.: Time-dependent entrainment of smoke presents an observational challenge for assessing aerosol-cloud interactions over the southeast Atlantic Ocean, Atmos. Chem. Phys., 18, https://doi.org/10.5194/acp-18-14623-2018, 2018.

Doherty, S. J., Saide, P. E., Zuidema, P., Shinozuka, Y., Ferrada, G. A., Gordon, H., Mallet, M., Meyer, K., Painemal, D., Howell, S. G., Freitag, S., Dobracki, A., Podolske, J. R., Burton, S. P., Ferrare, R. A., Howes, C., Nabat, P., Carmichael, G. R., Da Silva, A., … Redemann, J.: Modeled and observed properties related to the direct aerosol radiative effect of biomass burning aerosol over the southeastern Atlantic, Atmos. Chem. Phys., 22, https://doi.org/10.5194/acp-22-1-2022 , 2022.

Duncan Fairlie, T., Jacob, D. J., and Park, R. J.: The impact of transpacific transport of mineral dust in the United States, Atmos. Environ., 41, https://doi.org/10.1016/j.atmosenv.2006.09.048, 2007.

Faloona, I.: Sulfur processing in the marine atmospheric boundary layer: A review and critical assessment of modeling uncertainties, Atmos. Environ., 43, https://doi.org/10.1016/j.atmosenv.2009.02.043, 2009.

Formenti, P., Piketh, S. J., and Annegarn, H. J.: Detection of non-sea salt sulphate aerosol at a remote coastal site in South Africa: a PIXE study, Nucl. Instr. Meth. Phys. Res. B, 150, 332–338, https://doi.org/10.1016/S0168-583X(98)01041-6, 1999.

Formenti, P., D'Anna, B., Flamant, C., Mallet, M., Piketh, S. J., Schepanski, K., Waquet, F., Auriol, F., Brogniez, G., Burnet, F., Chaboureau, J. P., Chauvigné, A., Chazette, P., Denjean, C., Desboeufs, K., Doussin, J. F., Elguindi, N., Feuerstein, S., Gaetani, M., … Holben, B.: The aerosols, radiation and clouds in southern Africa field campaign in Namibia overview, illustrative observations, and way forward, B. Am. Meteorol. Soc., 100, 1277–1298, https://doi.org/10.1175/BAMS-D-17-0278.1, 2019.

Fountoukis, C., and Nenes, A.: ISORROPIA II: a computationally efficient thermodynamic equilibrium model for K+-Ca2+-Mg2+-NH4+ -Na+ -SO42− -NO3- - Cl- -H2O aerosols, Atmos. Chem. Phys, 7, 4639–4659, https://doi.org/10.5194/acp-7-4639-2007, 2007.

Fung, K. M., Heald, C. L., Kroll, J. H., Wang, S., Jo, D. S., Gettelman, A., Lu, Z., Liu, X., Zaveri, R. A., Apel, E. C., Blake, D. R., Jimenez, J.-L., Campuzano-Jost, P., Veres, P. R., Bates, T. S., Shilling, J. E., and Zawadowicz, M.: Exploring dimethyl sulfide (DMS) oxidation and implications for global aerosol radiative forcing, Atmos. Chem. Phys., 22, 1549–1573, https://doi.org/10.5194/acp-22-1549-2022, 2022.

Galí, M., Levasseur, M., Devred, E., Simó, R., and Babin, M.: Sea-surface dimethylsulfide (DMS) concentration from satellite data at global and regional scales, BG, 15, 3497–3519, https://doi.org/10.5194/bg-15-3497-2018, 2018.

Gantt, B., and Meskhidze, N.: The physical and chemical characteristics of marine primary organic aerosol: A review, Atmos. Chem. Phys., 13, 3979–3996, https://doi.org/10.5194/acp-13-3979-2013, 2013.

Gantt, B., Johnson, M. S., Crippa, M., Prévôt, A. S. H., and Meskhidze, N.: Implementing marine organic aerosols into the GEOS-Chem model, Geosci. Model Dev., 8, 619-629, https://doi.org/10.5194/gmd-8-619-2015, 2015.

Gelaro, R., McCarty, W., Suárez, M. J., Todling, R., Molod, A., Takacs, L., Randles, C. A., Darmenov, A., Bosilovich, M. G., Reichle, R., Wargan, K., Coy, L., Cullather, R., Draper, C., Akella, S., Buchard, V., Conaty, A., da Silva, A. M., Gu, W., … Zhao, B.: The modern-era retrospective analysis for research and applications, version 2 (MERRA-2), J. Climate, 30, 5419–5454, https://doi.org/10.1175/JCLI-D-16-0758.1, 2017.

Giles, D. M., Sinyuk, A., Sorokin, M. G., Schafer, J. S., Smirnov, A., Slutsker, I., Eck, T. F., Holben, B. N., Lewis, J. R., Campbell, J. R., Welton, E. J., Korkin, S. V., and Lyapustin, A. I.: Advancements in the Aerosol Robotic Network (AERONET) Version 3 database - Automated near-real-time quality control algorithm with improved cloud screening for Sun photometer aerosol optical depth (AOD) measurements, Atmos. Meas. Tech., 12, 169-209, https://doi.org/10.5194/amt-12-169-2019, 2019.

Gong, S. L.: A Parameterization of Sea-salt Aerosol Source Function for Sub- and Super-micron Particles. Glob. Biogeochem. Cycles, 17(4), https://doi.org/10.1029/2003GB002079, 2003.

Haywood, J. M., Abel, S. J., Barrett, P. A., Bellouin, N., Blyth, A., Bower, K. N., Brooks, M., Carslaw, K., Che, H., Coe, H., Cotterell, M. I., Crawford, I., Cui, Z., Davies, N., Dingley, B., Field, P., Formenti, P., Gordon, H., De Graaf, M., … Zuidema, P.: The CLoud-Aerosol-Radiation Interaction and Forcing: Year 2017 (CLARIFY-2017) measurement campaign, Atmos. Chem. Phys., 21, https://doi.org/10.5194/acp-21-1049-2021, 2021.

Hodzic, A., Campuzano-Jost, P., Bian, H., Chin, M., Colarco, P. R., Day, D. A., Froyd, K. D., Heinold, B., Jo, D. S., Katich, J. M., Kodros, J. K., Nault, B. A., Pierce, J. R., Ray, E., Schacht, J., Schill, G. P., Schroder, J. C., Schwarz, J. P., Sueper, D. T., … Jimenez, J. L.: Characterization of organic aerosol across the global remote troposphere: A comparison of ATom measurements and global chemistry models, Atmos. Chem. Phys., 20, https://doi.org/10.5194/acp-20-4607-2020, 2020.

Hoesly, R. M., Smith, S. J., Feng, L., Klimont, Z., Janssens-Maenhout, G., Pitkanen, T., Seibert, J. J., Vu, L., Andres, R. J., Bolt, R. M., Bond, T. C., Dawidowski, L., Kholod, N., Kurokawa, J. I., Li, M., Liu, L., Lu, Z., Moura, M. C. P., O'Rourke, P. R., and Zhang, Q.: Historical (1750-2014) anthropogenic emissions of reactive gases and aerosols from the Community Emissions Data System (CEDS), Geosci. Model Dev., 11(1), https://doi.org/10.5194/gmd-11-369-2018, 2018.

Hoffmann, E. H., Tilgner, A., Schrödner, R., Bräuer, P., Wolke, R., and Herrmann, H.: An advanced modeling study on the impacts and atmospheric implications of multiphase dimethyl sulfide chemistry, Proc. Natl. Acad. Sci. USA, 113, 11776–11781, https://doi.org/10.1073/pnas.1606320113, 2016.

Holben, B. N., Eck, T. F., Slutsker, I., Tanré, D., Buis, J. P., Setzer, A., Vermote, E., Reagan, J. A., Kaufman, Y. J., Nakajima, T., Lavenu, F., Jankowiak, I., and Smirnov, A.: AERONET - A federated instrument network and data archive for aerosol characterization, Remote Sens. Environ., 66, 1–16, https://doi.org/10.1016/S0034-4257(98)00031-5, 1998.

Hutchings, L., van der Lingen, C. D., Shannon, L. J., Crawford, R. J. M., Verheye, H. M. S., Bartholomae, C. H., van der Plas, A. K., Louw, D., Kreiner, A., Ostrowski, M., Fidel, Q., Barlow, R. G., Lamont, T., Coetzee, J., Shillington, F., Veitch, J., Currie, J. C., and Monteiro, P. M. S.: The Benguela Current: An ecosystem of four components, Prog. Oceanogr., 83, https://doi.org/10.1016/j.pocean.2009.07.046, 2009.

Jaeglé, L., Quinn, P. K., Bates, T. S., Alexander, B., and Lin, J. T.: Global distribution of sea salt aerosols: New constraints from in situ and remote sensing observations, Atmos. Chem. Phys., 11, https://doi.org/10.5194/acp-11-3137-2011, 2011.

Jaeglé, L., Shah, V., Thornton, J. A., Lopez-Hilfiker, F. D., Lee, B. H., McDuffie, E. E., Fibiger, D., Brown, S. S., Veres, P., Sparks, T. L., Ebben, C. J., Wooldridge, P. J., Kenagy, H. S., Cohen, R. C., Weinheimer, A. J., Campos, T. L., Montzka, D. D., Digangi, J. P., Wolfe, G. M., … Weber, R. J.: Nitrogen Oxides Emissions, Chemistry,

Deposition, and Export Over the Northeast United States During the WINTER Aircraft Campaign, J. Geophys. Res.-Atmos., 123, https://doi.org/10.1029/2018JD029133, 2018.

Jarre, A., Hutchings, L., Kirkman, S. P., Kreiner, A., Tchipalanga, P. C. M., Kainge, P., Uanivi, U., van der Plas, A. K., Blamey, L. K., Coetzee, J. C., Lamont, T., Samaai, T., Verheye, H. M., Yemane, D. G., Axelsen, B. E., Ostrowski, M., Stenevik, E. K., and Loeng, H.: Synthesis: Climate effects on biodiversity, abundance and distribution of marine organisms in the Benguela, Fish. Oceanogr., 24, https://doi.org/10.1111/fog.12086, 2015.

Kaiser, J. W., Heil, A., Andreae, M. O., Benedetti, A., Chubarova, N., Jones, L., Morcrette, J.-J, Razinger, M., Schultz, M. G., Suttie, M., and van der Werf, G. R.: Biomass burning emissions estimated with a global fire assimilation system based on observed fire radiative power, BG, 9, 527–554, https://doi.org/10.5194/bg-9-527-2012, 2012.

Kaufman, Y. J., and Tanré, D.: Effect of variations in super-saturation on the formation of cloud condensation nuclei, Nature, 369, 45-48, https://doi.org/10.1038/369045a0, 1994.

Kilgour, D. B., Novak, G. A., Sauer, J. S., Moore, A. N., Dinasquet, J., Amiri, S., Franklin, E. B., Mayer, K., Winter, M., Morris, C. K., Price, T., Malfatti, F., Crocker, D. R., Lee, C., Cappa, C. D., Goldstein, A. H., Prather, K. A., and Bertram, T. H.: Marine gas-phase sulfur emissions during an induced phytoplankton bloom, Atmos. Chem. Phys., 22, 1601–1613, https://doi.org/10.5194/acp-22-1601-2022, 2022.

Lana, A., Bell, T. G., Simó, R., Vallina, S. M., Ballabrera-Poy, J., Kettle, A. J., Dachs, J., Bopp, L., Saltzman, E. S., Stefels, J., Johnson, J. E., and Liss, P. S.: An updated climatology of surface dimethlysulfide concentrations and emission fluxes in the global ocean, Global Biogeochem. Cy., 25, https://doi.org/10.1029/2010GB003850, 2011.

Latimer, R. N. C., and Martin, R. V.: Interpretation of measured aerosol mass scattering efficiency over North America using a chemical transport model, Atmos. Chem. Phys., 19, https://doi.org/10.5194/acp-19-2635-2019, 2019.

Lee, G., Park, J., Jang, Y., Lee, M., Kim, K. R., Oh, J. R., Kim, D., Yi, H. Il, and Kim, T. Y.: Vertical variability of seawater DMS in the South Pacific Ocean and its implication for atmospheric and surface seawater DMS, Chemosphere, 78, 1063-1070, https://doi.org/10.1016/j.chemosphere.2009.10.054, 2010.

Lindesay, J. A., Andreae, M. O., Goldammer, J. G., Harris, G., Annegarn, H. J., Garstang, M., Scholes, R. J., and Van Wilgen, B. W.: International geosphere-biosphere programme/international global atmospheric chemistry SAFARI-92 field experiment: Background and overview, J. Geophys. Res., 101, https://doi.org/10.1029/96jd01512, 1996.

Martínez-Lozano, J. A., Utrillas, M. P., Tena, F., and Cachorro, V. E.: The parameterisation of the atmospheric aerosol optical depth using the Ångström power law, Sol. Energy, 63, 303–311, https://doi.org/10.1016/S0038-092X(98)00077-2, 1998.

Marvin, M. R., Palmer, P. I., Yao, F., Latif, M. T., and Khan, M. F.: Uncertainties from biomass burning aerosols in air quality models obscure public health impacts in Southeast Asia, Atmos. Chem. Phys., 24, 3699–3715. https://doi.org/10.5194/acp-24-3699-2024, 2024.

Middlebrook, A. M., Murphy, D. M., and Thomson, D. S.: Observations of organic material in individual marine particles at Cape Grim during the First Aerosol Characterization Experiment (ACE 1), J. Geophys. Res., 103, https://doi.org/10.1029/97JD03719, 1998.

Novak, G. A., Fite, C. H., Holmes, C. D., Veres, P. R., Neuman, J. A., Faloona, I., Thornton, J. A., Wolfe, G. M., Vermeuel, M. P., Jernigan, C. M., Peischl, J., Ryerson, T. B., Thompson, C. R., Bourgeois, I., Warneke, C., Gkatzelis, G. I., Coggon, M. M., Sekimoto, K., Bui, T. P., … Bertram, T. H.: Rapid cloud removal of dimethyl sulfide oxidation products limits SO2 and cloud condensation nuclei production in the marine atmosphere, Proc. Natl. Acad. Sci. USA, 118, https://doi.org/10.1073/pnas.2110472118, 2021.

O'Dowd, C. D., and De Leeuw, G.: Marine aerosol production: A review of the current knowledge, Phil. Trans. R. Soc. A., 365, 1753-1774, https://doi.org/10.1098/rsta.2007.2043, 2007.

O'Dowd, C. D., Facchini, M. C., Cavalli, F., Ceburnis, D., Mircea, M., Decesari, S., Fuzzi, S., Young, J. Y., and Putaud, J. P.: Biogenically driven organic contribution to marine aerosol, Nature, 431, https://doi.org/10.1038/nature02959, 2004.

Oppo, C., Bellandi, S., Degli Innocenti, N., Stortini, A. M., Loglio, G., Schiavuta, E., and Cini, R.: Surfactant components of marine organic matter as agents for biogeochemical fractionation and pollutant transport via marine aerosols, Mar. Chem., 63, 235–253, https://doi.org/10.1016/S0304-4203(98)00065-6, 1999.

Pai, S. J., Heald, C. L., Pierce, J. R., Farina, S. C., Marais, E. A., Jimenez, J. L., Campuzano-Jost, P., Nault, B. A., Middlebrook, A. M., Coe, H., Shilling, J. E., Bahreini, R., Dingle, J. H., and Vu, K.: An evaluation of global organic aerosol schemes using airborne observations, Atmos. Chem. Phys., 20, https://doi.org/10.5194/acp-20-2637-2020, 2020.

Park, R. J., Jacob, D. J., Chin, M., and Martin, R. V.: Sources of carbonaceous aerosols over the United States and implications for natural visibility, J. Geophys. Res., 108, https://doi.org/10.1029/2002jd003190, 2003.

Philip, S., Martin, R. V., and Keller, C. A.: Sensitivity of chemistry-transport model simulations to the duration of chemical and transport operators: A case study with GEOS-Chem v10-01, Geosci. Model Dev., 9, https://doi.org/10.5194/gmd-9-1683-2016, 2016.

Philip, S., Martin, R. V., Snider, G., Weagle, C. L., Van Donkelaar, A., Brauer, M., Henze, D. K., Klimont, Z., Venkataraman, C., Guttikunda, S. K., and Zhang, Q.: Anthropogenic fugitive, combustion and industrial dust is a significant, underrepresented fine particulate matter source in global atmospheric models, Environ. Res. Lett., 12, 044018, https://doi.org/10.1088/1748-9326/aa65a4, 2017.

Prather, K. A., Bertram, T. H., Grassian, V. H., Deane, G. B., Stokes, M. D., DeMott, P. J., Aluwihare, L. I., Palenik, B. P., Azam, F., Seinfeld, J. H., Moffet, R. C., Molina, M. J., Cappa, C. D., Geiger, F. M., Roberts, G. C., Russell, L. M., Ault, A. P., Baltrusaitis, J., Collins, D. B., … Zhao, D.: Bringing the ocean into the laboratory to probe the chemical complexity of sea spray aerosol, Proc. Natl. Acad. Sci. USA, 110, https://doi.org/10.1073/pnas.1300262110, 2013.

Quinn, P. K., and Bates, T. S. (2011).: The case against climate regulation via oceanic phytoplankton sulphur emissions, Nature, 480, 51–56, https://doi.org/10.1038/nature10580, 2011.

Quinn, P. K., Coffman, D. J., Johnson, J. E., Upchurch, L. M., and Bates, T. S.: Small fraction of marine cloud condensation nuclei made up of sea spray aerosol, Nat. Geosci., 10, https://doi.org/10.1038/ngeo3003, 2017.

Ravishankara, A. R., Rudich, Y., Talukdar, R., and Barone, S. B.: Oxidation of atmospheric reduced sulphur compounds: Perspective from laboratory studies, Philos. T. Roy. Soc. Lond. B., 352, 171–182, https://doi.org/10.1098/rstb.1997.0012, 1997.

Redemann, J., Wood, R., Zuidema, P., Doherty, S. J., Luna, B., LeBlanc, S. E., Diamond, M. S., Shinozuka, Y., Chang, I. Y., Ueyama, R., Pfister, L., Ryoo, J. M., Dobracki, A. N., da Silva, A. M., Longo, K. M., Kacenelenbogen, M. S., Flynn, C. J., Pistone, K., Knox, N. M., … Gao, L.: An overview of the ORACLES (ObseRvations of aerosols above CLouds and their intEractionS) project: Aerosol-cloud-radiation interactions in the southeast Atlantic basin, Atmos. Chem. Phys., 21, 1507–1563, https://doi.org/10.5194/acp-21-1507-2021, 2021.

Russell, L. M., Hawkins, L. N., Frossard, A. A., Quinn, P. K., and Bates, T. S.: Carbohydrate-like composition of submicron atmospheric particles and their production from ocean bubble bursting, Proc. Natl. Acad. Sci. USA, 107, https://doi.org/10.1073/pnas.0908905107, 2010.

Russell, L. M., Moore, R. H., Burrows, S. M., and Quinn, P. K.: Ocean flux of salt, sulfate, and organic components to atmospheric aerosol, Earth-Sci. Rev., 239, 10.1016/j.earscirev.2023.104364, 2023.

Ryoo, J. M., Pfister, L., Ueyama, R., Zuidema, P., Wood, R., Chang, I., and Redemann, J.: A meteorological overview of the ORACLES (ObseRvations of Aerosols above CLouds and their intEractionS) campaign over the southeastern Atlantic during 2016-2018: Part 1 – Climatology, Atmos. Chem. Phys., 21, 16689–16707, https://doi.org/10.5194/acp-21-16689-2021, 2021.

Seinfeld, J.H. and Pandis, S.N.: Atmos. Chem. Phys.: From Air Pollution to Climate Change. John Wiley and Sons, Hoboken, 2016.

Shannon, L. V., and Nelson, G.: The Benguela: Large Scale Features and Processes and System Variability, in: The South Atlantic, Springer, Berlin, Heidelberg, Germany, https://doi.org/10.1007/978-3-642-80353-6_9, 1996.

Spracklen, D. V., Carslaw, K. S., Kulmala, M., Kerminen, V. M., Sihto, S. L., Riipinen, I., Merikanto, J., Mann, G. W., Chipperfield, M. P., Wiedensohler, A., Birmili, W., and Lihavainen, H.: Contribution of particle formation to global cloud condensation nuclei concentrations, Geophys. Res. Lett., 35, https://doi.org/10.1029/2007GL033038, 2008.

Stier, P., Schutgens, N. A. J., Bellouin, N., Bian, H., Boucher, O., Chin, M., Ghan, S., Huneeus, N., Kinne, S., Lin, G., Ma, X., Myhre, G., Penner, J. E., Randles, C. A., Samset, B., Schulz, M., Takemura, T., Yu, F., Yu, H., and Zhou, C.: Host model uncertainties in aerosol radiative forcing estimates: Results from the AeroCom Prescribed intercomparison study, Atmos. Chem. Phys., 13, https://doi.org/10.5194/acp-13-3245-2013, 2013.

Su, M., Shi, Y., Yang, Y., and Guo, W.: Impacts of different biomass burning emission inventories: Simulations of atmospheric CO_2 concentrations based on GEOS-Chem, Sci. Total Environ., 876, https://doi.org/10.1016/j.scitotenv.2023.162825, 2023.

Swap, R., Garstang, M., Macko, S. A., Tyson, P. D., Maenhaut, W., Artaxo, P., Kållberg, P., and Talbot, R.: The long-range transport of southern African aerosols to the tropical South Atlantic, J. Geophys. Res., 101, https://doi.org/10.1029/95jd01049, 1996.

Swap, R. J., Annegarn, H. J., Suttles, J. T., King, M. D., Platnick, S., Privette, J. L., and Scholes, R. J.: Africa burning: A thematic analysis of the Southern African Regional Science Initiative (SAFARI 2000), J. Geophys. Res.-Atmos., 108, https://doi.org/10.1029/2003jd003747, 2003.

Tashmim, L., Porter, W. C., Chen, Q., Alexander, B., Fite, C. H., Holmes, C. D., Pierce, J. R., Croft, B., and Ishino, S.: Contribution of expanded marine sulfur chemistry to the seasonal variability of dimethyl sulfide oxidation products and size-resolved sulfate aerosol, Atmos. Chem. Phys., 24, https://doi.org/10.5194/acp-24-3379-2024, 2024.

Tortell, P.D., Guéguen, C., Long, M.C., Payne, C.D., Lee, P., and DiTullio, G.R.: Spatial variability and temporal dynamics of surface water pCO2, ΔO2/Ar and dimethylsulfide in the Ross Sea, Antarctica. Deep Sea Res. Part I Oceanogr. Res. Pap., 58, 241-259, https://doi.org/10.1016/j.dsr.2010.12.006, 2011.

Tournadre, J.: Anthropogenic pressure on the open ocean: The growth of ship traffic revealed by altimeter data analysis, Geophys. Res. Lett., 41, https://doi.org/10.1002/2014GL061786, 2014.

Van Der Werf, G. R., Randerson, J. T., Giglio, L., Collatz, G. J., Mu, M., Kasibhatla, P. S., Morton, D. C., Defries, R. S., Jin, Y., and Van Leeuwen, T. T.: Global fire emissions and the contribution of deforestation, savanna, forest, agricultural, and peat fires (1997-2009), Atmos. Chem. Phys., 10, https://doi.org/10.5194/acp-10-11707-2010, 2010.

Van Der Werf, G. R., Randerson, J. T., Giglio, L., Van Leeuwen, T. T., Chen, Y., Rogers, B. M., Mu, M., Van Marle, M. J. E., Morton, D. C., Collatz, G. J., Yokelson, R. J., and Kasibhatla, P. S.: Global fire emissions estimates during 1997-2016, Earth Syst. Sci. Data, 9, 697–720, https://doi.org/10.5194/essd-9-697-2017, 2017.

Veres, P. R., Andrew Neuman, J., Bertram, T. H., Assaf, E., Wolfe, G. M., Williamson, C. J., Weinzierl, B., Tilmes, S., Thompson, C. R., Thames, A. B., Schroder, J. C., Saiz-Lopez, A., Rollins, A. W., Roberts, J. M., Price, D., Peischl, J., Nault, B. A., Møller, K. H., Miller, D. O., … Ryerson, T. B.: Global airborne sampling reveals a

previously unobserved dimethyl sulfide oxidation mechanism in the marine atmosphere, Proc. Natl. Acad. Sci. USA, 117, https://doi.org/10.1073/pnas.1919344117, 2020.

Vignati, E., De Leeuw, G., and Berkowicz, R.: Modeling coastal aerosol transport and effects of surf-produced aerosols on processes in the marine atmospheric boundary layer, J. Geophys. Res., 106, https://doi.org/10.1029/2000JD000025, 2001.

Wang, X., Heald, C. L., Ridley, D. A., Schwarz, J. P., Spackman, J. R., Perring, A. E., Coe, H., Liu, D., and Clarke, A. D.: Exploiting simultaneous observational constraints on mass and absorption to estimate the global direct radiative forcing of black carbon and brown carbon, Atmos. Chem. Phys., 14, https://doi.org/10.5194/acp-14-10989-2014, 2014.

Wizenberg, T., Strong, K., Jones, D. B. A., Lutsch, E., Mahieu, E., Franco, B., and Clarisse, L.: Exceptional wildfire enhancements of PAN, C2H4, CH3OH, and HCOOH over the Canadian high Arctic during August 2017, J. Geophys. Res.-Atmos., 128, https://doi.org/10.1029/2022JD038052, 2023.

Wood, R.: Stratocumulus clouds, Mon. Weather Rev., 140, 2373–2423, https://doi.org/10.1175/MWR-D-11-00121.1, 2012.

Wu, R., Wang, S., and Wang, L.: New mechanism for the atmospheric oxidation of dimethyl sulfide. The importance of intramolecular hydrogen shift in a CH3SCH2OO radical, J. Phys. Chem. A, 119, 112–117, https://doi.org/10.1021/jp511616j, 2015.

Yu, F., Luo, G., and Ma, X.: Regional and global modeling of aerosol optical properties with a size, composition, and mixing state resolved particle microphysics model, Atmos. Chem. Phys., 12, https://doi.org/10.5194/acp-12-5719-2012, 2012.

Zhai, S., Jacob, D. J., Brewer, J. F., Li, K., Moch, J. M., Kim, J., Lee, S., Lim, H., Lee, H. C., Kuk, S. K., Park, R. J., Jeong, J. I., Wang, X., Liu, P., Luo, G., Yu, F., Meng, J., Martin, R. V., Travis, K. R., … Liao, H.: Relating geostationary satellite measurements of aerosol optical depth (AOD) over East Asia to fine particulate matter (PM2.5): insights from the KORUS-AQ aircraft campaign and GEOS-Chem model simulations, Atmos. Chem. Phys., 21, https://doi.org/10.5194/acp-21-16775-2021, 2021.

Zhang, D., Du, L., Wang, W., Zhu, Q., Bi, J., Scovronick, N., Naidoo, M., Garland, R.M. and Liu, Y.: A machine learning model to estimate ambient $PM_{2.5}$ concentrations in industrialized highveld region of South Africa, Remote Sens. Environ., 266, 112713, 2021.

Zuidema, P., Redemann, J., Haywood, J., Wood, R., Piketh, S., Hipondoka, M., and Formenti, P.: Smoke and clouds above the southeast Atlantic: Upcoming field campaigns probe absorbing aerosol's impact on climate, B. Am. Meteorol. Soc., 97, 1131–1135, https://doi.org/10.1175/BAMS-D-15-00082.1, 2016.

Zuidema, P., Alvarado, M., Chiu, C., de Szoeke, S., Fairall, C., Feingold, G., Freedman, A., Ghan, S., Haywood, J., Kollias, P., Lewis, E., McFarquhar, G., McComiskey, A., Mechem, D., Onasch, T., Redemann, J., Romps, D., Turner, D., Wang, H., Wood, R., Yuter, S., and Zhu, P.: Layered Atlantic Smoke Interactions with Clouds (LASIC) Field Campaign Report, United States, https://www.osti.gov/servlets/purl/1437446, 2018.